HHS Public Access

Author manuscript

Immunity. Author manuscript; available in PMC 2019 June 19.

Published in final edited form as:

Immunity. 2018 June 19; 48(6): 1245–1257.e9. doi:10.1016/j.immuni.2018.04.013.

Extrathymically generated regulatory T cells establish a niche for intestinal border-dwelling bacteria and affect physiologic metabolite levels

Clarissa Campbell[1,2,8], **Stanislav Dikiy**[1,2,8], **Shakti K. Bhattarai**[3,4], **Takatoshi Chinen**[1], **Fanny Matheis**[5], **Marco Calafiore**[6], **Beatrice Hoyos**[1], **Alan Hanash**[6,7], **Daniel Mucida**[5], **Vanni Bucci**[3], and **Alexander Y. Rudensky**[1,2,9]

[1]Howard Hughes Medical Institute and Immunology Program, Sloan Kettering Institute, and Ludwig Center at Memorial Sloan Kettering Cancer Center, New York, NY 10065, USA

[2]Immunology and Microbial Pathogenesis Program, Weill Cornell Graduate School of Medical Sciences, New York, NY 10021, USA

[3]Department of Biology, Program in Biotechnology and Biomedical Engineering, University of Massachusetts Dartmouth, MA, 02747, USA

[4]Department of Biology, Program in Engineering and Applied Science, University of Massachusetts Dartmouth, MA, 02747, USA

[5]Laboratory of Mucosal Immunology, The Rockefeller University, New York, NY 10065, USA

[6]Department of Medicine, Memorial Sloan Kettering Cancer Center, New York, NY 10065 USA

[7]Department of Medicine, Weill Cornell Medical College, New York, NY 10021 USA

[8]These authors contributed equally

[9]Lead contact

SUMMARY

The mammalian gut microbiota provides essential metabolites to the host and promotes the differentiation and accumulation of extrathymically generated regulatory T (pTreg) cells. To explore the impact of these cells on intestinal microbial communities, we assessed the composition of the microbiota in pTreg cell-deficient and -sufficient mice. pTreg cell deficiency led to

AUTHOR CONTRIBUTIONS

C.C., S.D., and A.Y.R. conceived the study, designed experiments and wrote the manuscript; C.C. and S.D. performed experiments and analyzed data; T.C. maintained GF mouse colony and assisted with multiplex cytokine assays; B.H. performed ELISAs for immunoglobulins; M.C. and A.H. performed analysis of intestinal crypt morphology and proliferation; F.M. and D.M. generated and analyzed images of mast cells in the intestines; S.K.B. and V.B. performed bioinformatics analyses on metabolomics data, bacterial whole-genome shotgun and 16S sequencing.

DATA AND SOFTWARE AVAILABILITY

IgA-Seq, metagenomics, and RNA-sequencing data are deposited in the BioProject database under accession: PRJNA438024.

Metabolomics data are included as Table S1.

heightened type 2 immune responses triggered by microbial exposure, which disrupted the niche of border dwelling bacteria early during colonization. Moreover, impaired pTreg cell generation led to pervasive changes in metabolite profiles, altered features of the intestinal epithelium and reduced body weight in the presence of commensal microbes. Absence of a single species of bacteria depleted in pTreg cell-deficient animals, *Mucispirillum schaedleri*, partially accounted for the sequelae of pTreg cell deficiency. These observations suggest that pTreg cells modulate the metabolic function of the intestinal microbiota by restraining immune defense mechanisms that may disrupt a particular bacterial niche.

Grapical Abstract

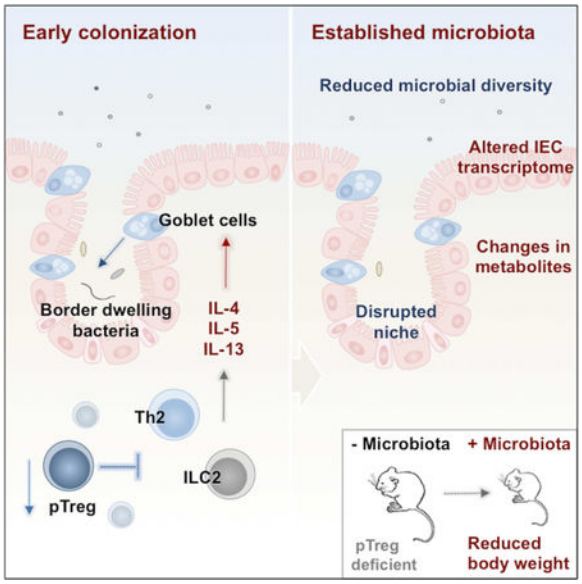

eTOC

Extrathymically generated regulatory (pTreg) cells are induced by bacterial products at mucosal sites. In this issue, Campbell and Dikiy et al. show that pTreg cell deficiency impedes the establishment of a subset of intestinal bacteria due to heightened immune response with significant effects on host metabolites and fitness (48 words)

INTRODUCTION

The emergence of major histocompatibility complex (MHC)-restricted recognition of antigens by $CD4^+$T cells enabled specific responses against microbes and non-infectious insults. Foxp3-expressing regulatory T (Treg) cells, a subset of $CD4^+$T cells, play a critical role as negative regulators of these immune responses. Treg cell ablation or loss-of-function mutations in the *Foxp3* gene disrupt peripheral tolerance, leading to a fatal multi-organ disease (Fontenot et al., 2003; Hori et al., 2003). Besides preventing transient impairment or permanent loss of tissue function by restraining exacerbated inflammation, Treg cells have been shown to directly partake in tissue repair upon injury (Arpaia et al., 2015; Burzyn et al.,

2013). Therefore, Treg cells serve as a key accessory cell type safeguarding tissue physiology and maintaining organismal homeostasis.

Although the majority of Treg cells are of thymic origin (tTreg cells), Foxp3 expression can also be induced in naïve $CD4^+$T cells in a manner dependent on the *Foxp3* intronic enhancer CNS1 (Zheng et al., 2010). In contrast to Treg cell ablation, which leads to systemic autoimmunity even in the absence of microbes (Chinen et al., 2010), selective impairment in extrathymically generated Treg (pTreg) cells results in age-dependent type 2 pathology restricted to mucosal sites (Josefowicz et al., 2012). Thus, the heterogeneity in Treg cell ontogeny may reflect a requirement for distinct antigenic specificity of tTreg and pTreg cells to support their divergent biological functions.

The mammalian gut harbors a complex microbial ecosystem that has co-evolved with its host to provide essential nutrients and support indispensable functions, including detoxification, colonization resistance, and immune defense (Sekirov et al., 2010). Being inherently foreign, the microbiota must engage immunoregulatory mechanisms during its establishment and maintenance to balance against its immunostimulatory capabilities. In support of this notion, it has been shown that microbial products including short chain fatty acids facilitate the differentiation of pTreg cells (Arpaia et al., 2013; Atarashi et al., 2011, 2013; Furusawa et al., 2013; Smith et al., 2013). Furthermore, pTreg cells recognizing commensal antigens are enriched in the colon (Lathrop et al., 2011; Nutsch et al., 2016). These observations suggest an important role for pTreg cells in maintaining a dynamic reciprocal relationship between the host intestinal epithelium and its microbiota and raise the question of whether these cells support the metabolic function of this “super organ”. We addressed this question by assessing the effect of pTreg cells on the composition of the intestinal microbiota and on the metabolome by comparing healthy pTreg cell-deficient mice ($Foxp3^{GFP\Delta CNS1}$) and their pTreg cell-sufficient littermates ($Foxp3^{GFP}$). Despite continuous bacterial exchange between co-housed animals, pTreg cell deficiency led to a focused perturbation in the composition of the microbiota, pervasive changes in luminal and circulating metabolites, and altered metabolic features of the intestinal epithelium. Heightened type 2 responses in hosts with impaired pTreg cell differentiation compromised the niche of a subset of border dwelling bacteria and diminished their abundance early during the process of community assembly. Removal of an abundant representative of these bacteria from a defined microbial consortium mirrored some key manifestations of pTreg cell deficiency that were observed in the presence of a complex microbiota. Our data suggest that pTreg cells shape the composition and metabolic function of intestinal microbial communities by suppressing immune defense mechanisms that would otherwise disrupt a particular microbial niche.

RESULTS

Genetic pTreg cell deficiency alters the intestinal microbial metagenome and depletes a subset of border dwelling bacteria

The finding that pTreg cell differentiation is promoted by microbial metabolites led us to ask whether pTreg cells reciprocally affect the composition of intestinal microbial communities and their metabolic function in physiological settings. To address this question, we took

advantage of *Foxp3*$^{GFP\Delta CNS1}$ mice, which carry a targeted deletion of the CNS1 enhancer in the *Foxp3* gene that leads to a selective deficiency in pTreg cell differentiation (Zheng et al., 2010). Since vertical transmission can confound the effects of host genetics on microbial ecology (Mamantopoulos et al., 2017), we set out to compare the microbial communities in *Foxp3*$^{GFP\Delta CNS1}$ and control *Foxp3*^{GFP} littermates maintained under specific pathogen-free (SPF) conditions (Figure 1A). To ensure that potential differences in the microbiota arose from ongoing host selection rather than vicariance, mutant and wild-type littermate mice were cohoused post-weaning. Furthermore, we restricted our study to 8 week-old mice to ensure that the observed effects were not a consequence of intestinal pathology, which may occur in older (6–8 month-old) *Foxp3*$^{GFP\Delta CNS1}$ animals (Josefowicz et al., 2012). Importantly, at this age *Foxp3*$^{GFP\Delta CNS1}$ mice were clinically healthy and showed no signs of overt inflammation as determined by histological analysis, fecal calprotectin levels and quantification of various inflammatory mediators in the serum and large intestine (Figure S1A-D). In order to detect changes caused by pTreg cell deficiency, we analyzed the cecal contents of 3 independent cohorts of mice by whole genome shotgun metagenomic sequencing. Numerous metabolic processes were underrepresented in the microbiota of *Foxp3*$^{GFP\Delta CNS1}$ mice, including the synthesis of several amino acids (Figure 1B). Purine biosynthesis and rhamnose degradation were among the few pathways enriched in the microbiota of *Foxp3*$^{GFP\Delta CNS1}$ animals (Figure 1B). The decreased abundance of several processes in the intestinal metagenome of *Foxp3*$^{GFP\Delta CNS1}$ mice raised the possibility that microbial pathways as a whole were less well represented in those animals. Indeed, microbial communities selected in pTreg cell-deficient hosts had reduced overall pathway coverage (Figure 1C), which may be accounted for by the decreased overall diversity of these communities (Figure 1D).

Next, we sought to determine the effect of pTreg cells on bacterial species composition. Microbial communities selected in *Foxp3*$^{GFP\Delta CNS1}$ hosts clustered separately from those selected in *Foxp3*^{GFP} mice (Figure 1D), showing significant decreases in *Lactobacillus johnsonii*, *Helicobacter hepaticus* and *Mucispirillum schaedleri*, and increases in *Alistipes sp.* and *Bacteroides uniformis* (Figure 1F). Although these bacteria were abundant in our colony (Figure S1E), their genetic contribution to significantly changed pathways was limited. With few exceptions, most differentially represented metabolic processes were contributed by bacteria whose differential abundance between host genotypes did not reach statistical significance in all experiments (Figure S1F). *L. johnsonii* and *M. schaedleri* are known to inhabit the intestinal mucus layer, and several *Helicobacter* species commonly establish close interaction with host epithelial cells; thus, impaired pTreg cell generation seems to adversely affect the niche of these “border occupants”, which may indirectly affect other members of microbial community through ecological interactions.

pTreg cells suppress type 2 responses triggered by microbial colonization

We assessed whether *de novo* assembly of microbial communities in pTreg cell-sufficient or deficient hosts could recapitulate our findings in the SPF setting. To best represent the microbial consortia that SPF *Foxp3*$^{GFP\Delta CNS1}$ and *Foxp3*^{GFP} mice were naturally exposed to, we transplanted germ-free (GF) animals via oral gavage with fresh fecal material collected from breeders that generated the SPF mice used in the experiments described above (see

experimental schematic in Figure 2A). Microbial communities selected in *Foxp3*$^{GFP\Delta CNS1}$ hosts showed reduced abundance of *M. schaedleri* and *H. hepaticus* (Figure S2A), indicating that the effect of pTreg cells in shaping the microbiota can be studied in a colonization setting and is not restricted to a particular developmental window. Knowing that conventionalization reproduced the effects of impaired pTreg cell differentiation on community composition, we then asked whether these changes begin to take place early after initial colonization. Mucus-penetrating *M. schaedleri* and *Akkermansia muciniphila* as well as another species of epsilonproteobacteria *Helicobacter ganmani* were already reduced in *Foxp3*$^{GFP\Delta CNS1}$ mice on day 7 (D7) post-conventionalization (Figure 2B), suggesting that pTreg cells modulate early events during community assembly, and therein, preserve the niche of these border dwellers.

Since the bacteria reduced in *Foxp3*$^{GFP\Delta CNS1}$ mice are known to inhabit the mucus layer or interact closely with host epithelial cells, we hypothesized that pTreg cells affected their niche by modulating the intestinal epithelium. To investigate this, we subjected the whole large intestine (LI) epithelial fraction to RNA-seq analysis. A small number of genes showed differential expression in the D7 LI epithelium, all more abundant in *Foxp3*$^{GFP\Delta CNS1}$ mice (Figure 2C). Notably, some of these genes encoded antimicrobial molecules (*Ang4, Retnlb, Itln1*) and others were associated with mucus production (*Fcgbp, Clca1*). Antimicrobial peptides are typically produced by Paneth cells, but can also be secreted by goblet cells (GCs), particularly in the LI (Bergstrom et al., 2015; Forman et al., 2012; Tsuji et al., 2010). Given the prominence of genes encoding antimicrobial molecules and mucus-related proteins in our dataset, we assessed the representation of GC signature transcripts using a previously published single-cell RNA sequencing analysis of intestinal epithelial cells (Yan et al., 2017). This analysis revealed that the GC signature was specifically enriched in *Foxp3*$^{GFP\Delta CNS1}$ mice (Figure 2D), suggesting heightened GC activation and/or increased representation of this lineage in the LI epithelium.

Type 2 cytokines are known to promote goblet cell activation and expansion. Th2 CD4$^+$ T cells and innate lymphoid cells type 2 (ILC2) serve as major producers of IL-4, IL-13, and IL-5 (Klein Wolterink et al., 2012; Neill et al., 2010; Price et al., 2010), and Treg cells have been suggested to limit both Th2 and ILC2 responses (Gasteiger et al., 2013a, 2013b, 2015; Molofsky et al., 2015). Flow cytometric analysis of cells isolated from the LI lamina propria (LP) showed increased production of IL-5 by ILC2 and IL-4 and IL-13 by CD4$^+$ T cells in *Foxp3*$^{GFP\Delta CNS1}$ mice relative to *Foxp3*^{GFP} controls, but not of other cytokines or by other cell types at D7 post-conventionalization (Figures 2E-F & S2B-E). Given the role of pTreg cells in restraining immune responses against dietary antigens (Kim et al., 2016), it was possible that these parameters differed between *Foxp3*$^{GFP\Delta CNS1}$ and *Foxp3*^{GFP} mice prior to microbial exposure. We found that the frequencies of ILC2 and effector T cells in GF *Foxp3*$^{GFP\Delta CNS1}$ and *Foxp3*^{GFP} controls were comparable (Figure 2G-H), indicating that the alterations on D7 arose from interactions with commensals. Moreover, mast cell accumulation was induced upon microbial colonization to a similar extent in *Foxp3*$^{GFP\Delta CNS1}$ and *Foxp3*^{GFP} mice (Figure S2F).

Interestingly, we also observed enhanced production of IL-13 by CD4$^+$ T cells in SPF *Foxp3*$^{GFP\Delta CNS1}$ mice (Figure S2G), suggesting that the “memory” of this heightened

immune response upon encounter with bacteria persists as immunological sequelae. Additionally, infiltration of mast cells remained increased in the LI of *Foxp3*$^{GFP\Delta CNS1}$ mice (Figure S2H), indicating that, although outwardly healthy, these animals presented sub-clinical type 2 immune responses.

Dysregulated type 2 responses disrupt the niche of border dwelling bacteria during the process of community assembly

To address the role of heightened early type 2 responses in precipitating the loss of border dwellers, we administered neutralizing antibodies (NAb) against IL-4, IL-5, and IL-13 or control IgG to GF *Foxp3*$^{GFP\Delta CNS1}$ and *Foxp3*^{GFP} animals during their conventionalization and analyzed microbial composition on D7 of colonization (see experimental schematic in Figure 3A). NAb treatment changed the abundance of a few microbial species in each genotype (Figure 3B) and remarkably restored the levels of *M. schaedleri* in *Foxp3*$^{GFP\Delta CNS1}$ animals to those observed in *Foxp3*^{GFP} controls (Figure 3C). Histological quantification of PAS-stained area in LI tissue sections showed a trend for GC expansion in the LI of *Foxp3*$^{GFP\Delta CNS1}$ mice compared to *Foxp3*^{GFP} controls in the isotype treated group, with both genotypes displaying a reduction upon NAb administration (Figure S3A). We used RT-qPCR to assess expression levels of *Ang4*, *Relmb* and *Clca1* in FACS-sorted GCs from the LI epithelium as markers of GC activation. Although the levels of *Relmb* and *Clca1* were similar between both genotypes regardless of treatment, *Ang4* expression was significantly increased in GCs from *Foxp3*$^{GFP\Delta CNS1}$ mice compared to *Foxp3*^{GFP} controls in the isotype group (Figure 3D). Furthermore, the levels of this transcript were reduced in both genotypes upon NAb treatment, suggesting that type 2 cytokines can modulate *Ang4* expression in GCs. Together, these data support the notion that type 2 cytokine-driven GC activation and expansion may contribute to the heightened GC responses in *Foxp3*$^{GFP\Delta CNS1}$ mice suggested by our RNA-seq data.

In addition to mucus and antimicrobial peptides, IgA forms the first line of defense in the intestinal mucosa. Although most intestinal bacteria are coated with polyreactive IgA produced independently of T cell help (Bunker et al., 2017), atypical commensals such as *Candidatus arthromitus* (Segmented Filamentous Bacteria) and *M. schaedleri* evade such responses and instead elicit T-cell dependent IgA secretion (Bunker et al., 2015). *Foxp3*$^{GFP\Delta CNS1}$ and *Foxp3*^{GFP} mice showed similar frequencies of germinal center B cells (Figure S3B) and IgA^{+} B cells (Figure S3C) in the Peyer's patches on D7 post-colonization, suggesting that the magnitude of IgA responses were comparable. To investigate potential qualitative differences in IgA responses, we performed 16S IgA-seq in *Foxp3*$^{GFP\Delta CNS1}$ and *Foxp3*^{GFP} mice as previously described (Kau et al., 2015) and compared the frequencies of bacteria in the sorted IgA^{+} fraction to their corresponding abundances in the whole community or input (Figure S3D). Notably, *Bacteroides acidifaciens* was the only species that showed differential enrichment in the IgA^{+} fraction between *Foxp3*^{GFP} and *Foxp3*$^{GFP\Delta CNS1}$ mice (Figure S3E), suggesting that divergent IgA responses are likely not driving the loss of border dwellers in the latter.

Collectively, our results show that pTreg cells ensure the establishment of border dwelling bacteria such as *M. schaedleri* during community assembly by suppressing early type 2

responses. Increased levels of type 2 cytokines enhanced GC responses, including the secretion of bactericidal molecules, likely making the niche inhospitable for certain microbes living in close proximity to host intestinal epithelium.

pTreg cell-deficiency leads to microbiota-driven changes in intestinal and circulating metabolites

Since microbial communities selected in hosts with impaired pTreg cell differentiation displayed reduced metabolic potential and diversity (Figure 1C-E), we decided to explore the effects of pTreg cells on metabolites by performing untargeted biochemical profiling of cecal contents and serum of *Foxp3*$^{GFP\Delta CNS1}$ and *Foxp3*^{GFP} mice by LC/MS and DSM/MS. Several classes of metabolites were markedly altered in abundance in both intestinal lumen and serum (Figure 4A). Remarkably, more than 80% (194 out of 225) of the significantly changed metabolites in the cecum were increased in *Foxp3*$^{GFP\Delta CNS1}$ mice compared to controls, and the inverse pattern was observed in the serum (82%, 67 out of 81 metabolites). Dipeptides containing essential amino acids were increased in the cecal contents from *Foxp3*$^{GFP\Delta CNS1}$ mice, while the levels molecules participating in glutathione (GSH) biosynthesis such as 5-oxoproline, glutamate and cysteine sulfinic acid were reduced in their sera (Table 1). Furthermore, various esterified lipids accumulated in the intestines of *Foxp3*$^{GFP\Delta CNS1}$ mice while the circulating levels of polyunsaturated fatty acids (PUFAs) were decreased (Table 1). Random Forest (RF) analysis identified various dipeptides amongst the most discriminatory compounds found in cecal contents, while nucleotide catabolites ranked highly in serum samples (Figure 4B). Of note, *Foxp3*$^{GFP\Delta CNS1}$ mice presented higher levels of S-adenosylhomocysteine (SAH) and trymethylene N-oxide (TMAO) (Table 1), increased abundance of which have been linked to cardiovascular disease (Tang et al., 2013; Xiao et al., 2015). Importantly, metabolite profiles in GF *Foxp3*$^{GFP\Delta CNS1}$ and *Foxp3*^{GFP} control animals were largely similar, with only a small number of lipids presenting the same differential pattern observed in SPF mice (Figure S4A). Combined, these analyses suggest that most changes observed in the SPF setting are driven, either directly or indirectly, by the commensal microbiota.

We next asked whether any of these alterations could be reproduced by using minimal microbial consortia designed to recapitulate the differences in the composition of the complex microbial communities selected in *Foxp3*$^{GFP\Delta CNS1}$ or *Foxp3*^{GFP} control mice. In designing these communities, we exploited the fact that one of the species consistently reduced in *Foxp3*$^{GFP\Delta CNS1}$ mice (*M. schaedleri*) is a component of the Altered Schaedler Flora (ASF), a limited consortium of 8 culturable bacterial strains used to approximate the function of a complete microbiota (Wymore Brand et al., 2015). We colonized GF *Foxp3*$^{GFP\Delta CNS1}$ and *Foxp3*^{GFP} mice with ASF with or without *M. schaedleri* (Figure 4C; referred to as ASF and ASF$^{\Delta 457}$, respectively) and 14 days post-colonization carried out metabolite profiling of the cecal contents and serum as described above. There were significant changes in the abundance of numerous circulating and luminal metabolites between the ASF and ASF$^{\Delta 457}$ groups (Figures 4D). These changes were largely consistent when comparing cohorts of ASF vs. ASF$^{\Delta 457}$ *Foxp3*$^{GFP\Delta CNS1}$ and *Foxp3*^{GFP} mice (Figure 4E), indicating that they could be attributed to the presence or absence of ASF457 regardless of host genotype. This was not the case for serum metabolites, possibly because at this early

time point the effects of the microbial composition on circulating metabolites have not propagated systemically. We then examined to what extent these differences paralleled those previously observed between *Foxp3*^{GFP} mice (which harbor *M. schaedleri*) and *Foxp3*$^{GFP\Delta CNS1}$ mice (which have reduced levels of this species). Projecting the significantly altered metabolites in the *Foxp3*$^{GFP\Delta CNS1}$ vs. *Foxp3*^{GFP} comparison onto volcano plots comparing ASF vs. ASF$^{\Delta 457}$ groups of either genotype showed that, even if not always reaching statistical significance, metabolite profiles in ASF$^{\Delta 457}$ mice approximated those in *Foxp3*$^{GFP\Delta CNS1}$ mice (Figure 4F and data not shown). Particularly, dipeptides enriched in the luminal contents of *Foxp3*$^{GFP\Delta CNS1}$ mice were enriched in ASF$^{\Delta 457}$ over ASF cohorts. Of note, *M. schaedleri* is predicted to rely heavily on protein and amino acids for carbon metabolism (Loy et al., 2017), harboring putative genes for 3 aminopeptidases, some of which predicted to be secreted.

Finally, to assess the effects of this representative border occupant on host immune responses, we characterized the immune cell composition of the intestinal tract of *Foxp3*$^{GFP\Delta CNS1}$ and *Foxp3*^{GFP} mice colonized with ASF or ASF$^{\Delta 457}$. As expected, there was a blunted expansion of Treg cells in the LI LP of *Foxp3*$^{GFP\Delta CNS1}$ mice compared to *Foxp3*^{GFP} mice regardless of the bacterial consortium (Figure S4B). Interestingly, the aberrant expansion of mucosal mast cells was only observed in *Foxp3*$^{GFP\Delta CNS1}$ mice colonized with ASF$^{\Delta 457}$, implying that this phenotype emerges as a consequence of the loss of ASF457 but only in a specific genetic context (Figure S4C). These data also reinforce the notion that the mast cell accumulation in *Foxp3*$^{GFP\Delta CNS1}$ mice is a consequence, rather than a cause of their altered microbiota. Furthermore, we did not observe changes in the effector T cell compartment caused by the presence of ASF457 in either genotype (Figure S4D-G), suggesting that differential *M. schaedleri*-specific T cell responses are unlikely driving the loss of this bacteria in *Foxp3*$^{GFP\Delta CNS1}$ mice. These results suggest that the absence of a single bacterial species, whose abundance is regulated by pTreg cells, can have profound effects on the intestinal metabolome.

Impaired pTreg cell generation affects intestinal and organismal homeostasis

Besides its role in directly providing metabolic services, the intestinal microbiota also imparts on host metabolism by regulating genes involved in nutrient uptake and energy homeostasis (Bäckhed et al., 2004; Turnbaugh et al., 2006). The inverse enrichment of many metabolites in the intestinal lumen versus in circulation was suggestive of functional alterations in the intestines of SPF *Foxp3*$^{GFP\Delta CNS1}$ mice; therefore, we sought to assess gene expression in the gut epithelium. RNA-seq analysis of the unfractionated epithelial layer revealed differential expression of several genes involved in nutrient uptake in the small intestine (Figure 5A, top left panel). Furthermore, gene ontology (GO) analysis showed enrichment of transcripts associated with metabolic and nutrient transport pathways in *Foxp3*$^{GFP\Delta CNS1}$ mice (Figure 5B). Gene expression analysis of the bulk epithelium of GF *Foxp3*$^{GFP\Delta CNS1}$ and *Foxp3*^{GFP} mice showed minimal changes in the levels of transcripts associated with these GO terms (Figure 5A, bottom left panel), suggesting that the intestinal microbiota drives functional metabolic changes in tissues of pTreg cell-deficient animals. Additionally, we detected increased levels of several transcripts associated with mast cells (*Cma2, Mcpt1, Mcpt2* and *Fcer1a*) in the LI epithelium of SPF (Figure 5A, top right panel),

but not GF (Figure 5A, bottom right panel) *Foxp3*$^{GFP\Delta CNS1}$ mice, corroborating our observation that microbial colonization drives sustained intestinal mast cell infiltration in animals lacking pTreg cells. To investigate whether pTreg cell deficiency had widespread effects on intestinal homeostasis, we further assessed other parameters of intestinal epithelium function. Serum endotoxin levels were comparable between SPF *Foxp3*$^{GFP\Delta CNS1}$ and *Foxp3*^{GFP} mice (Figure S5A), suggesting that intestinal barrier integrity was not altered. Histological assessment showed colonic crypt hyperplasia and increased cell proliferation in SPF *Foxp3*$^{GFP\Delta CNS1}$ mice compared to controls (Figure S5B and S5C), without significant alterations in the small intestine (data not shown). However, similar differences were also observed in GF *Foxp3*$^{GFP\Delta CNS1}$ and *Foxp3*^{GFP} mice (Figure S5B), suggesting that pTreg cells—likely induced in a CNS1-dependent manner in response to dietary antigens—can affect epithelial cell proliferation independently of the microbiota (Josefowicz et al., 2012). Overall, these results indicate that impaired pTreg cell generation selectively affects the metabolic function of the intestinal epithelium in the presence of commensal bacteria.

Finally, we asked whether these metabolic alterations resulted in additional organismal changes. Despite consuming similar amounts of food (Figure 5C), SPF *Foxp3*$^{GFP\Delta CNS1}$ mice had significantly lower body weights compared to *Foxp3*^{GFP} littermate controls (Figure 5D), indicating altered metabolic homeostasis and a potentially reduced capacity for energy harvest. Moreover, although GF *Foxp3*$^{GFP\Delta CNS1}$ and *Foxp3*^{GFP} mice had similar starting body weights (Figure S5D), pTreg cell-deficient animals showed delayed weight gain post-conventionalization (Figure 5E), implying impaired metabolic adaptation to the presence of intestinal commensals. Collectively, our studies suggest that pTreg cells significantly affect organismal homeostasis by promoting the optimal coordinated metabolic function of the microbiota and the intestinal epithelium.

DISCUSSION

The adaptive immune system has a remarkable ability for not only mounting protective responses against diverse pathogens but also for establishing tolerance towards a wide array of self and environmental antigens. The narrow scope of symbiotic relations between invertebrates and their microbiota suggests that this property of the adaptive immune system may have enabled the higher organisms to support complex microbial communities and abet their functions. Here, we uncovered a non-redundant role for pTreg cells during the assembly of intestinal microbial communities, placing this subset of adaptive lymphocytes as a key regulator of host-commensal interactions in mammalian hosts.

Our demonstration that impaired extrathymic generation of Treg cells in the absence of CNS1 leads to lasting and reproducible alterations in microbial composition is particularly significant since CNS1-deficient and control animals were littermates co-housed from birth and after weaning. Notably, Rag-deficient animals, which lack Treg cells as well as all other adaptive lymphocytes, harbor a microbiota distinct from Rag-sufficient animals, which cannot be entirely corrected by co-housing (Scholz et al., 2014; Zhang et al., 2015). The fact that we were able to largely reproduce these changes by colonizing adult germ-free mice with the same starting microbial inoculum reinforces the notion that a distinct microbiota is generated *de novo* due to altered selection of the community as a consequence of the CNS1

deficiency. Furthermore, microbial communities selected in hosts with pTreg cell-deficiency showed reduced diversity and coverage of metabolic pathways, highlighting the importance of these cells in regulating general properties of the intestinal microbiota. This diminished coverage cannot be readily attributed to specific bacteria in *Foxp3*$^{GFP\Delta CNS1}$ mice and is likely caused by the cumulative effects of subtle shifts in the abundance of numerous species. Therefore, the fact that we detected a limited number of species consistently altered in *Foxp3*$^{GFP\Delta CNS1}$ hosts may not only reflect the stringency of our analysis but could also imply that pTreg cells indirectly shape microbial communities by regulating the abundance of a few keystone bacteria.

Using conventionalization of GF mice to gain insight into how pTreg cells affect the establishment of commensal microbes, we showed that the loss of border dwelling bacteria happened shortly after colonization and was accompanied by increased GC responses. These responses included the secretion of bactericidal molecules, which could potentially make the niche inhospitable for certain microbes. Type 2 cytokines, particularly IL-4 and IL-13, are well-known inducers of goblet cell activation (Kondo et al., 2002; Zhu et al., 1999); indeed, *Foxp3*$^{GFP\Delta CNS1}$ mice exhibited heightened ILC2 and Th2 responses upon conventionalization. Neutralization of IL-4, IL-5 and IL-13 reduced GC activation and allowed for *M. schaedleri* to colonize pTreg cell-deficient hosts, showing that suppression of early type 2 responses is necessary and sufficient for the establishment of border dwellers. While other studies have suggested that pTreg cells specifically control ILC2 and T cell responses (Fontenot et al., 2003; Hori et al., 2003; Molofsky et al., 2015), exactly how pTreg cells suppress this early innate response remains to be determined.

Our characterization of the intestinal immune compartment of 8-week old SPF *Foxp3*$^{GFP\Delta CNS1}$ mice revealed that aspects of this heightened response to microbial colonization persist as immunological sequelae. We suggest that this skewing towards type 2 responses may eventually give rise to the overt allergy-like intestinal pathology observed in aged *Foxp3*$^{GFP\Delta CNS1}$ mice (Josefowicz et al., 2012). Interestingly, inclusion of *M. schaedleri* in a minimal microbial consortium normalized mast cell frequencies in *Foxp3*$^{GFP\Delta CNS1}$ mice, indicating that mast cell infiltration was subsequent to the loss of this bacterium and that prophylactic administration of microbes with similar properties may aid in preventing the development of allergic disease in susceptible hosts. In support of this notion, provision of another pTreg cell-dependent bacterium, *L. johnsonii*, was shown to limit type 2 allergic responses (Fujimura et al., 2014). Moreover, *H. hepaticus* was shown to induce an anti-inflammatory gene signature in healthy hosts (Danne et al., 2017), suggesting that pTreg cell-dependent bacteria identified in our study collectively contribute to the maintenance of intestinal homeostasis and the beneficial functions of the microbiota.

Although we have not directly assessed bacterial antigen-specific T cell responses, IgA-seq analyses in *Foxp3*$^{GFP\Delta CNS1}$ and *Foxp3*^{GFP} mice failed to reveal differences in IgA binding to *M. schaedleri* or other depleted bacteria. Since IgA responses to *M. schaedleri* are T cell-dependent (Bunker et al., 2015), a corollary of these results is that effector T cell responses against this bacterium are likely unaltered in pTreg cell-deficient animals. Furthermore, we were unable to detect changes in cytokine production by T cell in hosts colonized with defined microbial consortia with or without *M. schaedleri*. However, it seems likely that the

antigenic specificity of pTreg cells towards commensals may underlie their role in preserving the niche of border-dwelling bacteria, since *H. hepaticus* potently induces the accumulation of antigen-specific pTreg cells in the colon (Chai et al., 2017; Xu et al., 2018). Based on these results, we propose that pTreg cells are an essential intermediary of a circuit wherein common products of commensal origin suppress early immune responses triggered by microbial colonization and thereby preserve the integrity of microbial niches.

Our metabolome analysis demonstrated a profound effect of pTreg cells on intestinal and circulating metabolites, with broad changes in lipids and amino acids. Notably, *Foxp3*$^{GFP\Delta CNS1}$ mice showed a reduction in serum precursors for glutathione biosynthesis and intermediates of the urea cycle. Since di- and tri-peptides containing essential amino acids were enriched in the ceca of *Foxp3*$^{GFP\Delta CNS1}$ mice, we speculate that impaired uptake of these nutrients may cause systemic changes in nitrogen metabolism and potentially compromise redox homeostasis in these animals. Alterations in amino acid-related compounds were only present in SPF animals, indicating that intestinal microbes—either by modulating host responses or through direct metabolic activity—are required for these changes to manifest. In agreement with this notion, our metabolomics analyses of minimal microbial communities designed to reproduce the effect of the presence or absence of a representative pTreg cell-dependent border dweller (*M. schaedleri*) recapitulated the accumulation of peptides in cecal contents. Furthermore, *Foxp3*$^{GFP\Delta CNS1}$ mice exhibited increased levels of SAH and TMAO, two molecules strongly associated with predisposition for cardiovascular disease. These observations suggest that besides promoting the uptake of important nutrients, pTreg cells can potentially affect organismal physiology by reducing the levels of harmful compounds.

Foxp3$^{GFP\Delta CNS1}$ mice also exhibited reduced weight in comparison to their *Foxp3*^{GFP} mice littermates. This effect was dependent on microbial colonization, since GF *Foxp3*$^{GFP\Delta CNS1}$ mice had comparable body weights to their littermate controls but fell markedly behind in gaining weight after conventionalization. Additionally, maladaptive responses to colonization also manifested as altered gene expression in the intestinal epithelium of SPF *Foxp3*$^{GFP\Delta CNS1}$ animals. Jointly, these findings indicate a prominent role for pTreg cells in enhancing host fitness by promoting the optimal functioning of the “super organ” comprising the intestine and the microbiota.

Overall, our data strongly support the conclusion that most of the phenotypic sequelae of pTreg cell deficiency emerge either early as a direct consequence of a dysregulated immune responses to the microbiota or over time due to alterations in the microbial communities. We suggest that the loss of border dwelling bacteria drives various other phenotypic differences caused by pTreg cell deficiency, since the presence or absence of a single affected bacterial species (*M. schaedleri*) recapitulates numerous discrepancies between *Foxp3*$^{GFP\Delta CNS1}$ and *Foxp3*^{GFP} mice. These observations may in part explain the seeming discordance between the focused microbial alterations in *Foxp3*$^{GFP\Delta CNS1}$ mice and the profound alterations in host physiology and immune status. Altogether, our study revealed a substantial effect of pTreg cells on the metabolic state of the host under physiologic conditions and suggests that microbiota-driven generation of pTreg cells serves as an essential feedback mechanism affecting the composition and function of microbial communities.

STAR Methods

CONTACT FOR REAGENT AND RESOURCE SHARING

Further information and requests for resources and reagents should be directed to and will be fulfilled by the Lead Contact, Alexander Rudensky (rudenska@mskcc.org).

EXPERIMENTAL MODEL AND SUBJECT DETAILS

Mice

SPF animals: Animals were housed in an SPF facility with 12-hour light/dark cycles under ambient conditions and with *ad libitum* access to food and water. Institutional health reports indicate the presence of a *Tritrichomonad* protozoan, segmented filamentous bacteria, and *Helicobacter spp.* in our mouse colony. Harem breeding with *Foxp3*$^{GFP/GFP\Delta CNS1}$ female mice and *Foxp3*^{GFP} or *Foxp3*^{GFPDTR} males were fed the Breeder diet (5058) and generated experimental male *Foxp3*^{GFP} (RRID: MGI:3574978) and *Foxp3*$^{GFP\Delta CNS1}$ (RRID: MGI: 4430239) littermates. Experimental mice were weaned to ensure co-housing of genotypes and switched to a standard rodent diet (5053).

GF animals: For re-derivation, *Foxp3*$^{GFP\Delta CNS1}$ and *Foxp3*^{GFP} pups were delivered by sterile cesarean section and fostered by germ-free dams. GF animals were maintained in flexible isolators (Class Biologically Clean; USA) at Weill Cornell Medicine and fed with autoclaved 5KA1 chow. GF status was routinely checked by aerobic and anaerobic cultures of fecal samples for bacteria and fungi and by PCR of fecal DNA samples for bacterial 16S and fungal/yeast 18S genes.

All animals: All mice were housed at the Research Animal Resource Center for Memorial Sloan Kettering Cancer Center and Weill Cornell Medicine. All studies were under protocol 08–10-023 and approved by the Sloan Kettering Institute Institutional Animal Care and Use Committee. All strains were backcrossed at least 10 times to the C57BL6/J background. Male mice were used for all experiments; since the Foxp3 gene is X-linked, female littermates of differing genotypes could not be generated. SPF animals were always 8 weeks of age at analysis and GF and ex-GF mice were at least 8 weeks old at the initiation of experiments. All animals used in this study had no previous history of experimentation and were naïve at the time of analysis.

Details as to the experimental grouping of animals are addressed in the Quantification and Statistical Analysis section.

Bacteria—ASF bacteria were grown under anaerobic conditions in supplemented BHI medium as previously described (Biggs et al., 2017). Frozen stocks of individual ASF strains were streaked on supplemented BHI agar plates [250mL of deionized water, 250mL of tap water, 18.5g of BBL™ BHI (BD Biosciences, 299070), 6.5g of Bacto™ agar (BD Biosciences, 214010), 2.5g of Bacto™ Yeast extract (BD Biosciences, 288620), 0.1 mL of vitamin K1 (Millipore Sigma, 95271) stock solution (1% vitamin K1 in absolute ethanol, stored at −80°C), 0.25mL of hemin (Millipore Sigma, 51280) stock solution (10mg/mL), 0.25g cysteine (Gibco, 810–1033IM), 25mL of FBS (ThermoFisher, 35010CV), 25mL of

horse serum (ThermoFisher, 26050088) and 25mL sheep serum (Millipore Sigma, S2263)] and incubated in the anaerobic chamber at 37°C until growth was visible. Plates were kept moist by daily addition of 100uL of sterile reduced PBS to support the growth of fastidious strains.

METHOD DETAILS

Details as to the experimental grouping of animals, sample size, replicates, and inclusion/exclusion of data are addressed in the Quantification and Statistical Analysis section.

Conventionalization—Freshly collected feces from *Foxp3*$^{GFP/GFP\Delta CNS1}$ female and *Foxp3*^{GFP} or *Foxp3*^{GFPDTR} male breeders used to generate experimental SPF mice were manually homogenized in 1mL of sterile PBS. Solid material from the fecal homogenate was removed by brief centrifugation at low speed. 100uL of a 2-fold dilution of this fecal slurry was administered to GF *Foxp3*$^{GFP\Delta CNS1}$ and *Foxp3*^{GFP} animals by gavage. Animals were individually housed after conventionalization for the periods indicated.

Colonization with ASF—ASF bacteria were scraped from agar plates with bacteriological loops into sterile anaerobic PBS. Consortia were mixed in an anaerobic chamber, transported in airtight tubes to the animal facility, and quickly administered to experimental animals by oral gavage. Mice were manipulated using aseptic techniques inside sterile biosafety cabinets and housed in autoclaved cages for the duration of the experiments.

Neutralizing antibody (NAb) treatment—25μg each of anti-mouse IL-4 (11B.11), anti-mouse IL-13 (8H8) and anti-mouse IL-5 (TRFK5) in 100μl sterile PBS were administered i.p. at 24 hours before and again at the moment of conventionalization (described above). Mice were also injected with 50μg of each antibody in 200μl PBS 3 days after conventionalization. ‘Isotype controls’ were treated with equivalent doses of rat IgG1 and mouse IgG1 of irrelevant specificity.

Whole genome shotgun and 16S metagenomic sequencing of intestinal microbiota—Cecal/fecal DNA was extracted using the E.Z.N.A stool DNA kit according to manufacturer’s instructions. For amplicon sequencing, the V4 region of the bacterial 16S gene was amplified from 10–50ng of DNA using KOD hot start DNA polymerase and barcoded primers (Caporaso et al., 2011). Libraries were size-selected with AMPure XP magnetic beads and sequenced on the Illumina MiSeq platform using the V3 600 cycle kit. Libraries for whole genome shotgun sequencing were prepared with the Nextera XT kit according to manufacturer’s protocol and sequenced on a HiSeq platform (paired-end 100bp at a depth of 15–20 million reads/sample) by the Integrated Genomics Operation (iGO) core facility at MSKCC.

Bioinformatics analyses of microbial communities—For the analysis of shotgun metagenomic reads, sequences were first trimmed and removed of host contamination using Trimmomatic and Bowtie2. Host-decontaminated reads were then profiled for microbial species abundances using MetaPhlAn and for abundance of UniRef gene and KEGG

orthologs, and functional pathways (MetaCyc pathways, KEGG pathways, and KEGG modules) using the software pipeline HUMAnN2 and in-house written scripts (available upon request). Normalized taxonomic, gene, and pathway abundances were then used for downstream statistical analysis in R. Tables with bacterial, genes or pathways abundances were imported into R as phyloseq objects. Differential analysis to determine bacterial species and microbial functional pathways differential between *Foxp3*$^{GFP\Delta CNS1}$ and *Foxp3*^{GFP} littermate controls was performed using LefSE. Features with p value <0.05 for the class-level Kruskall-Wallis (KW) test and, analogously, with p-value <0.05 in the sub-class level Mann-Whitney (MW) U test were determined as significant. Only features that displayed the same enrichment profile among all experiments were retained. Shannon diversity for bacterial and pathway abundance was determined using the function available in the R phyloseq package. Testing for differential diversity between *Foxp3*$^{GFP\Delta CNS1}$ and *Foxp3*^{GFP} littermate controls was performed using a linear regression model Diversity ~ Genotype + Exp. Replicate. Diversity was considered statistically different between *Foxp3*$^{GFP\Delta CNS1}$ and *Foxp3*^{GFP} samples if the p-value associated to differences in Genotype was smaller than 0.05. Analysis of 16S sequencing data was performed with QIIME.

Metabolite profiling—Blood was collected in serum separator tubes (Becton Dickinson, 365967) after terminal bleeding by cardiac puncture. Blood was allowed to clot for 1–2 hours at room temperature. Sera were then isolated by centrifugation at 13,000xg for 3 minutes and transferred to new tubes. Sera and cecal contents were snap-frozen in liquid N_2 and stored at −80°C until analysis. Unbiased profiling of lipids and water-soluble metabolites was carried out by Metabolon, Inc. For the analysis of global metabolite profiling, tables with scaled normalized abundances (obtained from Metabolon) were imported into R as phyloseq objects. Metabolites differentially abundant between *Foxp3*$^{GFP\Delta CNS1}$ and *Foxp3*^{GFP} controls were determined by MW U test, with p-value <0.05. Random Forest Analysis was performed to identify metabolites with predictive power to correctly assign samples into *Foxp3*$^{GFP\Delta CNS1}$ or *Foxp3*^{GFP} groups. The R package randomForest was used to build 1500 decision trees. Metabolites were ranked for importance to classification according to the resulting associated Mean Decreased Accuracy.

Mast cell imaging in intestinal tissues—Formalin-fixed whole mount intestinal sections from *Foxp3*$^{GFP\Delta CNS1}$ and *Foxp3*^{GFP} animals were stained using rabbit anti-mouse GFP Alexa Fluor 488, Rat anti-mouse Mcpt1 and rat anti-mouse EpCAM (CD326) Alexa-Fluor 647 antibodies. Images were acquired on an inverted Leica DMI 6000 microscope (Leica, Germany) and are representative of 2 mice per group. Data were analyzed using Imaris software.

Intestinal crypt measurements, EdU incorporation, and PAS quantification—Tissues from relevant animals were resected and placed in 10% formalin. The intestinal lumen was gently flushed with 10% formalin. Histological processing and Hematoxylin and eosin (H&E) as well as Alcian-Blue/Periodic acid–Schiff stain (PAS/AB) staining of intestinal tissues was carried out by the Molecular Cytology Core at MSKCC using a Discovery XT processor (Ventana Medical Systems). For crypt measurement and EdU quantification, animals were injected with EdU (50mg/kg) intraperitoneally 24 hours before

analysis. Detection of EdU was performed with Click-iT® Plus EdU Proliferation Kits per manufacturer instructions. H&E stained sections were scanned and automated measurements of crypt length were done with ImageJ. PAS/AB sections were scanned at and automated quantification was carried by the Histology and Imaging Core at the University of Washington.

Isolation of cells from intestinal epithelia, lamina propria, and Peyer's patches—For RNA-sequencing and flow cytometric analyses, 12cm of the terminal ileum and the combined cecum and colon were processed as the small intestine and large intestine, respectively. Organs were resected and the Peyer's patches and cecal patch were removed. Organs were then defatted, opened longitudinally and luminal contents were removed by vigorous manual shaking of the tissue in PBS. Tissues were then cut into 1–2 cm pieces and incubated in 25mL IEL solution [1x PBS w/ 2% FBS (ThermoFisher, 35010CV), 10mM HEPES buffer (ThermoFisher, MT 25–060-CI), 1% penicillin/streptomycin (ThermoFisher, MT 30–002-CI), 1% L-glutamine (ThermoFisher, MT 25–005-CI), plus 1mM EDTA (Sigma, E4884) and 1mM DTT (Sigma, D9779) added immediately before use] for 15 minutes at 37°C with vigorous shaking (250rpm). After centrifugation (450g, 5 minutes) cells and tissue were resuspended in wash buffer (1x RPMI 1640 w/2% FBS, 10mM HEPES buffer, 1% penicillin/streptomycin, 1% L-glutamine) by vortexing. Epithelial and immune cells from the epithelial layer were collected by pouring suspension through a 100μm strainer (ThermoFisher, 07–201-432). Remaining tissue was then incubated in 25mL collagenase solution [wash buffer w/0.2U/mL collagenase A (Sigma, 11088793001) and 1U/mL DNase I (Sigma, 10104159001)] for 30 minutes at 37°C with vigorous shaking (250rpm). ¼inch ceramic beads (MP Biomedicals, 116540034) were added to large intestine samples (3–4 per sample) to aid in tissue disassociation. Digested samples were then passed through a 100μm strainer and centrifuged to remove collagenase solution. Lamina propria samples were washed by centrifugation in 40% Percoll™ (ThermoFisher, 45–001-747) in PBS to remove debris and enrich for leukocytes. All samples were washed by centrifugation in 5–10mL wash buffer. For RNA-sequencing, $1/5^{th}$ of the cells collected as the epithelial fraction (mixed epithelial and immune cells) were ressuspended in 1mL Trizol™ and snap-frozen in liquid N_2. Peyer's patches were resected from the ileum and mechanically dissociated with the plunger end of a 3mL syringe in wash buffer. The resulting single cell suspension was passed through a 100μm nylon mesh.

Flow cytometric analysis of cytokine production—To assess cytokine production after *ex vivo* restimulation, single cell suspensions were incubated for 3 hours at 37°C with 5% CO_2 in the presence of 50ng/mL PMA and 500 ng/mL ionomycin with 1 μg/mL brefeldin A and 2μM monensin to inhibit ER and Golgi transport. For flow cytometric analysis, cells were first washed with cold PBS and then stained with Ghost Dye™ Violet 510 or Ghost Dye™ Red 780 in PBS for 10 minutes at 4°C to aid in excluding dead cells. Cells were then incubated with anti-CD16/32 in staining buffer [0.1% (w/v) BSA (VWR, 97061–422), 2mM EDTA, 10mM HEPES in 1x PBS] for 15 minutes at 4°C to block binding to Fc receptors. Extracellular antigens were stained for 25 minutes at 4°C in staining buffer. Cells were fixed and permeabilized with BD Cytofix/Cytoperm (for cytokine restimulations) or ThermoFisher Transcription Factor Fix/Perm (for transcription factor staining) per

manufacturer instructions. Intracellular antigens were stained for 1 hour at 4°C in the appropriate 1x Perm/Wash buffer. Cells were washed with staining buffer and passed through a 100μm nylon mesh before acquisition on a BD LSR II (Becton Dickinson). 123count eBeads™ were added at 2500 beads/sample to quantify absolute cell numbers.

Sorting of goblet cells and RT-qPCR—Single cell suspensions of the LI epithelial fraction were stained for sorting of goblet cells as previously described (Hrvatin et al., 2014; Knoop et al., 2015) with some modifications. Cells were stained for live/dead discrimination and extracellular antigens as described above. Cells were fixed with 4% PFA and permeabilized with 0.1% (w/v) saponin in PBS supplemented with 400U/mL RRI at 4°C for 30 minutes. Cells were washe d with Wash Buffer [0.2% (w/v) BSA, 0.1% (w/v) saponin, 400U/mL RRI in 1x PBS] and centrifuged at 1000xg for 5 minutes. Cells were stained with 1:100 anti-Cytokeratin 18 antibody in Wash Buffer for 1 hour at 4°C with gentle rotation on an orbital shaker. Cells were washed as before and then stained with secondary antibody (anti-mouse pan IgG) as before. Cells were washed with Staining Buffer (see flow cytometric section above) supplemented with RRI and resuspended in the same for sorting. GCs were identified as $EpCAM^{+}CD45^{-}CD24^{-}UEA\text{-}I^{+}CK\text{-}18^{+}$ and 5,000–25,000 cells per mouse were sorted directly into Trizol-LS™.

Later, Trizol™ samples for bulk IECs and sorted GCs were allowed to thaw and supplemented with 200μl Chloroform (Sigma-Aldrich, C2432). Samples were manually shaken and then aqueous phase was separated by centrifugation for 15 minutes at 13,000xg at 4°C in Phase Lock Heavy tubes (Quantabio, 2302830). Aqueous phase was transferred to new 1.5mL tubes and mixed with 600μl 2-propanol and 3μl GlycoBlue™ Coprecipitant (Thermo Fisher, AM9516). RNA was allowed to precipitate at −20°C for 1 hour before centrifugation for 10 minutes at 13,000xg at 4°C. RNA pellet was washed twice with 1 mL 75% ethanol before being allowed to air-dry and resuspended in 20–100μl Nuclease-free H_2O (Thermo Fisher, AM9932). Reverse transcription was carried out with Superscript VILO IV master mix according to manufacturer instructions. qPCR reactions were set up in 384-well format in 10μl using Power SYBR™ Green PCR Master Mix following manufacturer instructions. PCR was carried out on an Applied Biosystems 7900HT instrument using default settings. Primers were designed using the IDT design tool and validated before use by dissociation curve analysis. Primers were designed to span an exon-exon junction of the transcripts assessed. Length of products ranged from 90 to 110 base pairs. CT values for 3 technical replicates per probe, per sample were averaged and used to generate $2^{\Delta CT}$ normalized to *Villin* transcripts on a per mouse basis.

Sorting and 16S rRNA sequencing of IgA-coated bacteria (IgA-seq)—IgA-Seq was carried out as described (Kau et al., 2015), with some modifications. Fresh fecal pellets were mechanically dissociated in 500μl of sterile PBS. Larger particles were removed by centrifugation at 400xg for 2 minutes. Supernatant was transferred to a new tube and centrifuged at 5000xg for 5 minutes to pellet bacteria. Pellets were resuspended in 300μl sterile-filtered staining buffer (flow cytometry section) and 50μl were transferred to 96-well V-bottom plates for staining. Bacteria were resuspended in 50μl of staining buffer with 1:50 PE anti-mouse IgA and stained for 15 minutes at 4°C. Bacter ia were washed by addition of

150μl of staining buffer and centrifugation at 1000xg for 10 minutes. Bacteria were resuspended in 400μl staining buffer supplemented with 1:1000 Syto BC. Bacteria were sorted on a BD Aria II with the threshold set to 200 on SSC. FSC and SSC were acquired on a logarithmic scale. Bacteria were gated by FSC and SSC and then as Syto BC^+. 50,000–100,000 IgA^+ events were sorted as the 'IgA^+' fraction, and 100,000 Syto BC^+ events (irrespective of $IgA^{+/-}$) were sorted as 'input'. Sorted bacteria were frozen at −80°C for future DNA extraction.

Analysis of IgA-sequencing data—16S rRNA libraries for the 'input' and 'IgA^+' fractions were analyzed using QIIME. The resulting OTU table was imported in R. For each OTU we used DESeq2 to fit the model $NC_i \sim$ Genotype + Treatment + Genotype: Treatment. Here NC_i is the DESeq2-normalized counts for each OTU_i, Genotype corresponds to *Foxp3*$^{GFP\Delta CNS1}$ and *Foxp3*^{GFP} and Treatment to 'Input' vs. 'IgA^+' fraction. We used an adjusted p-value (Benjamin-Hochberg) of 0.05 to determine OTUs that were differentially abundant (a) between Input and IgA^+ fractions in *Foxp3*^{GFP}, (b) between Input and IgA^+ fractions in *Foxp3*$^{GFP\Delta CNS1}$ and (c) between Input and IgA^+ fraction in a genotype-dependent manner.

RNA-sequencing experiments—RNA was extracted from Trizol™ and prepared for sequencing by the Integrated Genomics Core at Memorial Sloan Kettering Cancer Center. 10–30 million 50bp paired-end reads were acquired on an Illumina HiSeq 2000. Reads were aligned to the GRCm38 mouse genome assembly using hisat2 and counted using htseq with default parameters. Differential expression analysis was performed using edgeR. Data were plotted using R and ggplot2 (Wickham, 2009). Goblet cell genes were defined as those significantly enriched in 'cluster 9' in Yan et al., 2017. For Gene Ontology (GO) analysis, the GOrilla tool was used. Genes significantly differentially expressed (>0.5 log2 FC, <0.05 adjusted P-value), split as significantly under or overexpressed, were used as target sets. Genes with mean expression > $\log_2(3)$ normalized counts were used as the background set.

Multiplex cytokine measurements and ELISAs—Fecal calproctectin levels were determined by ELISA using the S100A9/Calprotectin Mouse kit. Briefly, stool was homogeneized in extraction buffer [0.1 M Tris, 0.15 M NaCl, 1.0 M urea, 10 mM $CaCl_2$, 0.1 M citric acid monohydrate, 5 g/L BSA, pH 8.0] at 100 mg/mL and vortexed at maximum speed for 10 minutes. Diluted supernatants were used for ELISA according to manufacturer's protocol. For multiplex cytokine assay, whole intestinal tissue was snap-frozen in liquid N_2. Tissue was then thawed into 200μl Cell extraction buffer supplemented with cOmplete mini protease inhibitor tablets and 1mM PMSF. Tissues were homogenized in Soft Tissue homogenizing tubes with a Bead Ruptor 24 (Biotage) [Output: 6, On time: 30 sec, Off time: 5 sec, Cycles: 4]. After centrifugation to remove particulate debris, total protein was quantified using a Bradford assay (ThermoFisher, 23200). A custom ProcartaPlex 18-plex assay was carried out according to manufacturer instructions and read on a Luminex 200 (Luminex Corp) instrument. Standard curves were generated and values interpolated using R. Serum IgA concentrations were measured using SBA Clonotyping System-HRP per manufacturer instructions. IgE was quantified using biotinylated anti-IgE

detection antibody (BD Pharmingen,553414) and streptavidin-conjugated HRP. ELISAs were read at OD 450 on a Synergy HTX instrument (BioTek).

QUANTIFICATION AND STATISTICAL ANALYSIS—Analysis of RNA-sequencing, IgA-Seq, metagenomics, and metabolomics data including statistical testing were carried out in R as specified in the relevant sections in Method Details. Analysis of flow cytometric data was carried out in FlowJo. Statistical analysis of flow cytometric and all other data were performed in Prism.

Details as to number of replicates sample size, significance tests, definition of center, dispersion and precision measures, and value and meaning of n for each experiment are included in the accompanying figure legends. All experiments, excluding RNA-sequencing, were carried out independently at least twice. Mice were non-randomly allocated to experimental groups to ensure equal distribution of genotypes between treatments. Researchers were not blinded as to genotype or treatment during the experiments. No measures were taken to estimate sample size of to determine whether the data met the assumptions of the statistical approaches used. Significance (α) was defined as <0.05 throughout, after correcting for multiple comparisons.

*Exclusion of outliers for SPF mice.

Supplementary Material

Refer to Web version on PubMed Central for supplementary material.

ACKNOWLEDGEMENTS

We thank Drs. Alessandra Piersigilli (MSKCC) and Piper Treuting (University of Washington) for pathological assessment of histological specimens, Aneta Rogoz (Rockefeller University) for re-derivation of GF mouse strains, Dr. Michael Wannemuehler (Iowa State University) for ASF bacterial strains, Eric Pamer (MSKCC) for assistance with anaerobic bacterial culture and all the members of the Rudensky lab for technical support and discussion. This work was supported by NIH/NCI Cancer Center Support Grant (CCSG) P30CA008748, NIH grant R37AI034206, the Ludwig Center at Memorial Sloan Kettering, the Hilton-Ludwig Cancer Prevention Initiative (Conrad N. Hilton Foundation and Ludwig Cancer Research). A.Y.R is an investigator with the Howard Hughes Medical Institute. V.B. acknowledges support by the National Institute of Allergy and Infectious Disease Grant R15-AI112985–01A1 and the National Science Foundation Grant 1458347).

REFERENCES

Abubucker S, Segata N, Goll J, Schubert AM, Izard J, Cantarel BL, Rodriguez-Mueller B, Zucker J, Thiagarajan M, Henrissat B, et al. (2012). Metabolic reconstruction for metagenomic data and its application to the human microbiome. PLoS Comput. Biol 8, e1002358. [PubMed: 22719234]

Anders S, Pyl PT, and Huber W (2015). HTSeq--a Python framework to work with high-throughput sequencing data. Bioinforma. Oxf. Engl 31, 166–169.

Liaw Andy, and Wiener Matthew (2002). Classification and Regression by randomForest. R News 2, 18–22.

Arpaia N, Campbell C, Fan X, Dikiy S, van der Veeken J, deRoos P, Liu H, Cross JR, Pfeffer K, Coffer PJ, et al. (2013). Metabolites produced by commensal bacteria promote peripheral regulatory T-cell generation. Nature 504, 451–455. [PubMed: 24226773]

Arpaia N, Green JA, Moltedo B, Arvey A, Hemmers S, Yuan S, Treuting PM, and Rudensky AY (2015). A Distinct Function of Regulatory T Cells in Tissue Protection. Cell 162, 1078–1089. [PubMed: 26317471]

Atarashi K, Tanoue T, Shima T, Imaoka A, Kuwahara T, Momose Y, Cheng G, Yamasaki S, Saito T, Ohba Y, et al. (2011). Induction of colonic regulatory T cells by indigenous Clostridium species. Science 331, 337–341. [PubMed: 21205640]

Atarashi K, Tanoue T, Oshima K, Suda W, Nagano Y, Nishikawa H, Fukuda S, Saito T, Narushima S, Hase K, et al. (2013). Treg induction by a rationally selected mixture of Clostridia strains from the human microbiota. Nature 500, 232–236. [PubMed: 23842501]

Bäckhed F, Ding H, Wang T, Hooper LV, Koh GY, Nagy A, Semenkovich CF, and Gordon JI (2004). The gut microbiota as an environmental factor that regulates fat storage. Proc. Natl. Acad. Sci. U. S. A 101, 15718–15723. [PubMed: 15505215]

Bergstrom KSB, Morampudi V, Chan JM, Bhinder G, Lau J, Yang H, Ma C, Huang T, Ryz N, Sham HP, et al. (2015). Goblet Cell Derived RELM-β Recruits CD4+ T Cells during Infectious Colitis to Promote Protective Intestinal Epithelial Cell Proliferation. PLoS Pathog 11, e1005108. [PubMed: 26285214]

Biggs MB, Medlock GL, Moutinho TJ, Lees HJ, Swann JR, Kolling GL, and Papin JA (2017). Systems-level metabolism of the altered Schaedler flora, a complete gut microbiota. ISME J 11, 426–438. [PubMed: 27824342]

Bolger AM, Lohse M, and Usadel B (2014). Trimmomatic: a flexible trimmer for Illumina sequence data. Bioinforma. Oxf. Engl 30, 2114–2120.

Bunker JJ, Flynn TM, Koval JC, Shaw DG, Meisel M, McDonald BD, Ishizuka IE, Dent AL, Wilson PC, Jabri B, et al. (2015). Innate and Adaptive Humoral Responses Coat Distinct Commensal Bacteria with Immunoglobulin A. Immunity 43, 541–553. [PubMed: 26320660]

Bunker JJ, Erickson SA, Flynn TM, Henry C, Koval JC, Meisel M, Jabri B, Antonopoulos DA, Wilson PC, and Bendelac A (2017). Natural polyreactive IgA antibodies coat the intestinal microbiota. Science 358.

Burzyn D, Kuswanto W, Kolodin D, Shadrach JL, Cerletti M, Jang Y, Sefik E, Tan TG, Wagers AJ, Benoist C, et al. (2013). A special population of regulatory T cells potentiates muscle repair. Cell 155, 1282–1295. [PubMed: 24315098]

Caporaso JG, Kuczynski J, Stombaugh J, Bittinger K, Bushman FD, Costello EK, Fierer N, Peña AG, Goodrich JK, Gordon JI, et al. (2010). QIIME allows analysis of high-throughput community sequencing data. Nat. Methods 7, 335–336. [PubMed: 20383131]

Caporaso JG, Lauber CL, Walters WA, Berg-Lyons D, Lozupone CA, Turnbaugh PJ, Fierer N, and Knight R (2011). Global patterns of 16S rRNA diversity at a depth of millions of sequences per sample. Proc. Natl. Acad. Sci. U. S. A 108 Suppl 1, 4516–4522. [PubMed: 20534432]

Chai JN, Peng Y, Rengarajan S, Solomon BD, Ai TL, Shen Z, Perry JSA, Knoop KA, Tanoue T, Narushima S, et al. (2017). Helicobacter species are potent drivers of colonic T cell responses in homeostasis and inflammation. Sci. Immunol 2.

Chinen T, Volchkov PY, Chervonsky AV, and Rudensky AY (2010). A critical role for regulatory T cell-mediated control of inflammation in the absence of commensal microbiota. J. Exp. Med 207, 2323–2330. [PubMed: 20921284]

Danne C, Ryzhakov G, Martínez-López M, Ilott NE, Franchini F, Cuskin F, Lowe EC, Bullers SJ, Arthur JSC, and Powrie F (2017). A Large Polysaccharide Produced by Helicobacter hepaticus Induces an Anti-inflammatory Gene Signature in Macrophages. Cell Host Microbe 22, 733–745. e5. [PubMed: 29241040]

Eden E, Lipson D, Yogev S, and Yakhini Z (2007). Discovering motifs in ranked lists of DNA sequences. PLoS Comput. Biol 3, e39. [PubMed: 17381235]

Eden E, Navon R, Steinfeld I, Lipson D, and Yakhini Z (2009). GOrilla: a tool for discovery and visualization of enriched GO terms in ranked gene lists. BMC Bioinformatics 10, 48. [PubMed: 19192299]

Fontenot JD, Gavin MA, and Rudensky AY (2003). Foxp3 programs the development and function of CD4+CD25+ regulatory T cells. Nat. Immunol 4, 330–336. [PubMed: 12612578]

Fontenot JD, Rasmussen JP, Williams LM, Dooley JL, Farr AG, and Rudensky AY (2005). Regulatory T cell lineage specification by the forkhead transcription factor foxp3. Immunity 22, 329–341. [PubMed: 15780990]

Forman RA, deSchoolmeester ML, Hurst RJM, Wright SH, Pemberton AD, and Else KJ (2012). The goblet cell is the cellular source of the anti-microbial angiogenin 4 in the large intestine post Trichuris muris infection. PloS One 7, e42248. [PubMed: 22970115]

Fujimura KE, Demoor T, Rauch M, Faruqi AA, Jang S, Johnson CC, Boushey HA, Zoratti E, Ownby D, Lukacs NW, et al. (2014). House dust exposure mediates gut microbiome Lactobacillus enrichment and airway immune defense against allergens and virus infection. Proc. Natl. Acad. Sci. U. S. A 111, 805–810. [PubMed: 24344318]

Furusawa Y, Obata Y, Fukuda S, Endo TA, Nakato G, Takahashi D, Nakanishi Y, Uetake C, Kato K, Kato T, et al. (2013). Commensal microbe-derived butyrate induces the differentiation of colonic regulatory T cells. Nature 504, 446–450. [PubMed: 24226770]

Gasteiger G, Hemmers S, Firth MA, Le Floc'h A, Huse M, Sun JC, and Rudensky AY (2013a). IL-2-dependent tuning of NK cell sensitivity for target cells is controlled by regulatory T cells. J. Exp. Med 210, 1167–1178. [PubMed: 23650441]

Gasteiger G, Hemmers S, Bos PD, Sun JC, and Rudensky AY (2013b). IL-2-dependent adaptive control of NK cell homeostasis. J. Exp. Med 210, 1179–1187. [PubMed: 23650439]

Gasteiger G, Fan X, Dikiy S, Lee SY, and Rudensky AY (2015). Tissue residency of innate lymphoid cells in lymphoid and nonlymphoid organs. Science 350, 981 –985. [PubMed: 26472762]

Hori S, Nomura T, and Sakaguchi S (2003). Control of regulatory T cell development by the transcription factor Foxp3. Science 299, 1057–1061. [PubMed: 12522256]

Hrvatin S, Deng F, O'Donnell CW, Gifford DK, and Melton DA (2014). MARIS: Method for Analyzing RNA following Intracellular Sorting. PLOS ONE 9, e89459. [PubMed: 24594682]

Jergens AE, Wilson-Welder JH, Dorn A, Henderson A, Liu Z, Evans RB, Hostetter J, and Wannemuehler MJ (2007). Helicobacter bilis triggers persistent immune reactivity to antigens derived from the commensal bacteria in gnotobiotic C3H/HeN mice. Gut 56, 934–940. [PubMed: 17145736]

Josefowicz SZ, Niec RE, Kim HY, Treuting P, Chinen T, Zheng Y, Umetsu DT, and Rudensky AY (2012). Extrathymically generated regulatory T cells control mucosal TH2 inflammation. Nature 482, 395–399. [PubMed: 22318520]

Kau AL, Planer JD, Liu J, Rao S, Yatsunenko T, Trehan I, Manary MJ, Liu T-C, Stappenbeck TS, Maleta KM, et al. (2015). Functional characterization of IgA-targeted bacterial taxa from undernourished Malawian children that produce diet-dependent enteropathy. Sci. Transl. Med 7, 276ra24.

Kim D, Langmead B, and Salzberg SL (2015). HISAT: a fast spliced aligner with low memory requirements. Nat. Methods 12, 357–360. [PubMed: 25751142]

Kim JM, Rasmussen JP, and Rudensky AY (2007). Regulatory T cells prevent catastrophic autoimmunity throughout the lifespan of mice. Nat. Immunol 8, 191–197. [PubMed: 17136045]

Kim KS, Hong S-W, Han D, Yi J, Jung J, Yang B-G, Lee JY, Lee M, and Surh CD (2016). Dietary antigens limit mucosal immunity by inducing regulatory T cells in the small intestine. Science 351, 858–863. [PubMed: 26822607]

Klein Wolterink R.G.J., Kleinjan A, van Nimwegen M, Bergen I, de Bruijn M, Levani Y, and Hendriks RW (2012). Pulmonary innate lymphoid cells are major producers of IL-5 and IL-13 in murine models of allergic asthma. Eur. J. Immunol 42, 1106–1116. [PubMed: 22539286]

Knoop KA, McDonald KG, McCrate S, McDole JR, and Newberry RD (2015). Microbial sensing by goblet cells controls immune surveillance of luminal antigens in the colon. Mucosal Immunol 8, 198–210. [PubMed: 25005358]

Kondo M, Tamaoki J, Takeyama K, Nakata J, and Nagai A (2002). Interleukin-13 induces goblet cell differentiation in primary cell culture from Guinea pig tracheal epithelium. Am. J. Respir. Cell Mol. Biol 27, 536–541. [PubMed: 12397012]

Langmead B, and Salzberg SL (2012). Fast gapped-read alignment with Bowtie 2. Nat. Methods 9, 357–359. [PubMed: 22388286]

Lathrop SK, Bloom SM, Rao SM, Nutsch K, Lio C-W, Santacruz N, Peterson DA, Stappenbeck TS, and Hsieh C-S (2011). Peripheral education of the immune system by colonic commensal microbiota. Nature 478, 250–254. [PubMed: 21937990]

Love MI, Huber W, and Anders S (2014). Moderated estimation of fold change and dispersion for RNA-seq data with DESeq2. Genome Biol 15, 550. [PubMed: 25516281]

Loy A, Pfann C, Steinberger M, Hanson B, Herp S, Brugiroux S, Gomes Neto J.C., Boekschoten MV, Schwab C, Urich T, et al. (2017). Lifestyle and Horizontal Gene Transfer-Mediated Evolution of Mucispirillum schaedleri, a Core Member of the Murine Gut Microbiota. mSystems 2.

Mamantopoulos M, Ronchi F, Van Hauwermeiren F, Vieira-Silva S, Yilmaz B, Martens L, Saeys Y, Drexler SK, Yazdi AS, Raes J, et al. (2017). Nlrp6- and ASC-Dependent Inflammasomes Do Not Shape the Commensal Gut Microbiota Composition. Immunity 47, 339–348. e4. [PubMed: 28801232]

McMurdie PJ, and Holmes S (2013). phyloseq: an R package for reproducible interactive analysis and graphics of microbiome census data. PloS One 8, e61217. [PubMed: 23630581]

Molofsky AB, Van Gool F, Liang H-E, Van Dyken SJ, Nussbaum JC, Lee J, Bluestone JA, and Locksley RM (2015). Interleukin-33 and Interferon-γ Counter-Regulate Group 2 Innate Lymphoid Cell Activation during Immune Perturbation. Immunity 43, 161–174. [PubMed: 26092469]

Neill DR, Wong SH, Bellosi A, Flynn RJ, Daly M, Langford TKA, Bucks C, Kane CM, Fallon PG, Pannell R, et al. (2010). Nuocytes represent a new innate effector leukocyte that mediates type-2 immunity. Nature 464, 1367–1370. [PubMed: 20200518]

Nutsch K, Chai JN, Ai TL, Russler-Germain E, Feehley T, Nagler CR, and Hsieh C-S (2016). Rapid and Efficient Generation of Regulatory T Cells to Commensal Antigens in the Periphery. Cell Rep 17, 206–220. [PubMed: 27681432]

Price AE, Liang H-E, Sullivan BM, Reinhardt RL, Eisley CJ, Erle DJ, and Locksley RM (2010). Systemically dispersed innate IL-13-expressing cells in type 2 immunity. Proc. Natl. Acad. Sci. U. S. A 107, 11489–11494. [PubMed: 20534524]

R Development Core Team (2011). R: A Language and Environment for Statistical Computing (Vienna, Austria : the R Foundation for Statistical Computing)

Robinson MD, McCarthy DJ, and Smyth GK (2010). edgeR: a Bioconductor package for differential expression analysis of digital gene expression data. Bioinforma. Oxf. Engl 26, 139–140.

Scholz F, Badgley BD, Sadowsky MJ, and Kaplan DH (2014). Immune mediated shaping of microflora community composition depends on barrier site. PloS One 9, e84019. [PubMed: 24416190]

Segata N, Waldron L, Ballarini A, Narasimhan V, Jousson O, and Huttenhower C (2012). Metagenomic microbial community profiling using unique clade-specific marker genes. Nat. Methods 9, 811–814. [PubMed: 22688413]

Sekirov I, Russell SL, Antunes LCM, and Finlay BB (2010). Gut microbiota in health and disease. Physiol. Rev 90, 859–904. [PubMed: 20664075]

Smith PM, Howitt MR, Panikov N, Michaud M, Gallini CA, Bohlooly-Y M, Glickman JN, and Garrett WS (2013). The microbial metabolites, short-chain fatty acids, regulate colonic Treg cell homeostasis. Science 341, 569–573. [PubMed: 23828891]

Tang WHW, Wang Z, Levison BS, Koeth RA, Britt EB, Fu X, Wu Y, and Hazen SL (2013). Intestinal Microbial Metabolism of Phosphatidylcholine and Cardiovascular Risk. N. Engl. J. Med 368, 1575–1584. [PubMed: 23614584]

Tsuji S, Tsuura Y, Morohoshi T, Shinohara T, Oshita F, Yamada K, Kameda Y, Ohtsu T, Nakamura Y, and Miyagi Y (2010). Secretion of intelectin-1 from malignant pleural mesothelioma into pleural effusion. Br. J. Cancer 103, 517–523. [PubMed: 20628387]

Turnbaugh PJ, Ley RE, Mahowald MA, Magrini V, Mardis ER, and Gordon JI (2006). An obesity-associated gut microbiome with increased capacity for energy harvest. Nature 444, 1027–1031. [PubMed: 17183312]

Wickham H (2009). ggplot2: Elegant Graphics for Data Analysis (Springer-Verlag New York)

Wymore Brand M., Wannemuehler MJ, Phillips GJ, Proctor A, Overstreet A-M, Jergens AE, Orcutt RP, and Fox JG (2015). The Altered Schaedler Flora: Continued Applications of a Defined Murine Microbial Community. ILAR J 56, 169–178. [PubMed: 26323627]

Xiao Y, Su X, Huang W, Zhang J, Peng C, Huang H, Wu X, Huang H, Xia M, and Ling W (2015). Role of S-adenosylhomocysteine in cardiovascular disease and its potential epigenetic mechanism. Int. J. Biochem. Cell Biol 67, 158–166. [PubMed: 26117455]

Xu M, Pokrovskii M, Ding Y, Yi R, Au C, Harrison OJ, Galan C, Belkaid Y, Bonneau R, and Littman DR (2018). c-MAF-dependent regulatory T cells mediate immunological tolerance to a gut pathobiont. Nature 554, 373–377. [PubMed: 29414937]

Yan KS, Janda CY, Chang J, Zheng GXY, Larkin KA, Luca VC, Chia LA, Mah AT, Han A, Terry JM, et al. (2017). Non-equivalence of Wnt and R-spondin ligands during Lgr5(+) intestinal stem-cell self-renewal. Nature 545, 238–242. [PubMed: 28467820]

Zhang H, Sparks JB, Karyala SV, Settlage R, and Luo XM (2015). Host adaptive immunity alters gut microbiota. ISME J 9, 770–781. [PubMed: 25216087]

Zheng Y, Josefowicz S, Chaudhry A, Peng XP, Forbush K, and Rudensky AY (2010). Role of conserved non-coding DNA elements in the Foxp3 gene in regulatory T-cell fate. Nature 463, 808–812. [PubMed: 20072126]

Zhu Z, Homer RJ, Wang Z, Chen Q, Geba GP, Wang J, Zhang Y, and Elias JA (1999). Pulmonary expression of interleukin-13 causes inflammation, mucus hypersecretion, subepithelial fibrosis, physiologic abnormalities, and eotaxin production. J. Clin. Invest 103, 779–788. [PubMed: 10079098]

Highlights (#characters):

- pTreg cells affect the intestinal microbiota composition in healthy mice
- pTreg cells suppress type 2 responses and preserve a border dwelling bacteria niche
- pTreg cell-dependent border dwelling bacteria affect the host metabolome
- pTreg cells promote organismal homeostasis in the presence of commensal bacteria

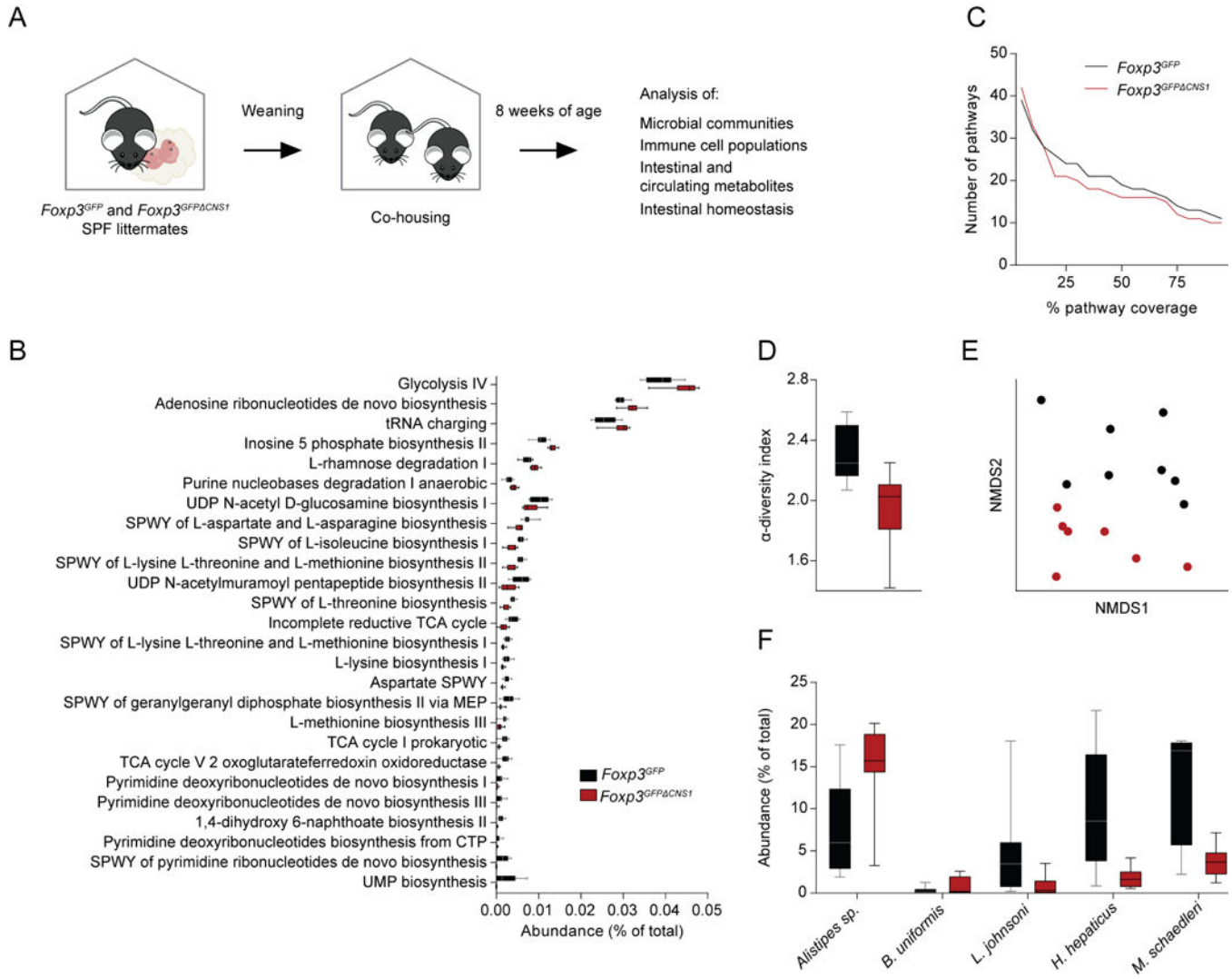

Figure 1. Properties of microbial communities selected in hosts with impaired pTreg cell generation.

(A) Schematic of experimental design. Multiple cohorts of *Foxp3*$^{GFP\Delta CNS1}$ and *Foxp3*^{GFP} WT littermate controls were co-housed post-weaning until analysis at 8 weeks of age. (B-F) Shotgun metagenomic sequencing of cecal contents. (B) Abundance of significantly altered microbial pathways. (C) Comparison of overall coverage of microbial pathways. (D) Shannon index for α-diversity. (E) β-diversity of intestinal microbial communities. Nonmetric Multidimensional Scaling (NMDS) representation of the Bray-Curtis index. (F) LEfSe analysis of bacterial abundance. Data in all panels are pooled from 3 independent experiments (n = 2–3 mice per group in each experiment). Error bars represent the median with min–max range. (B, F) Showing only significantly altered pathways/bacteria ($p<0.05$ KW test/MW U-test). See also Figure S1.

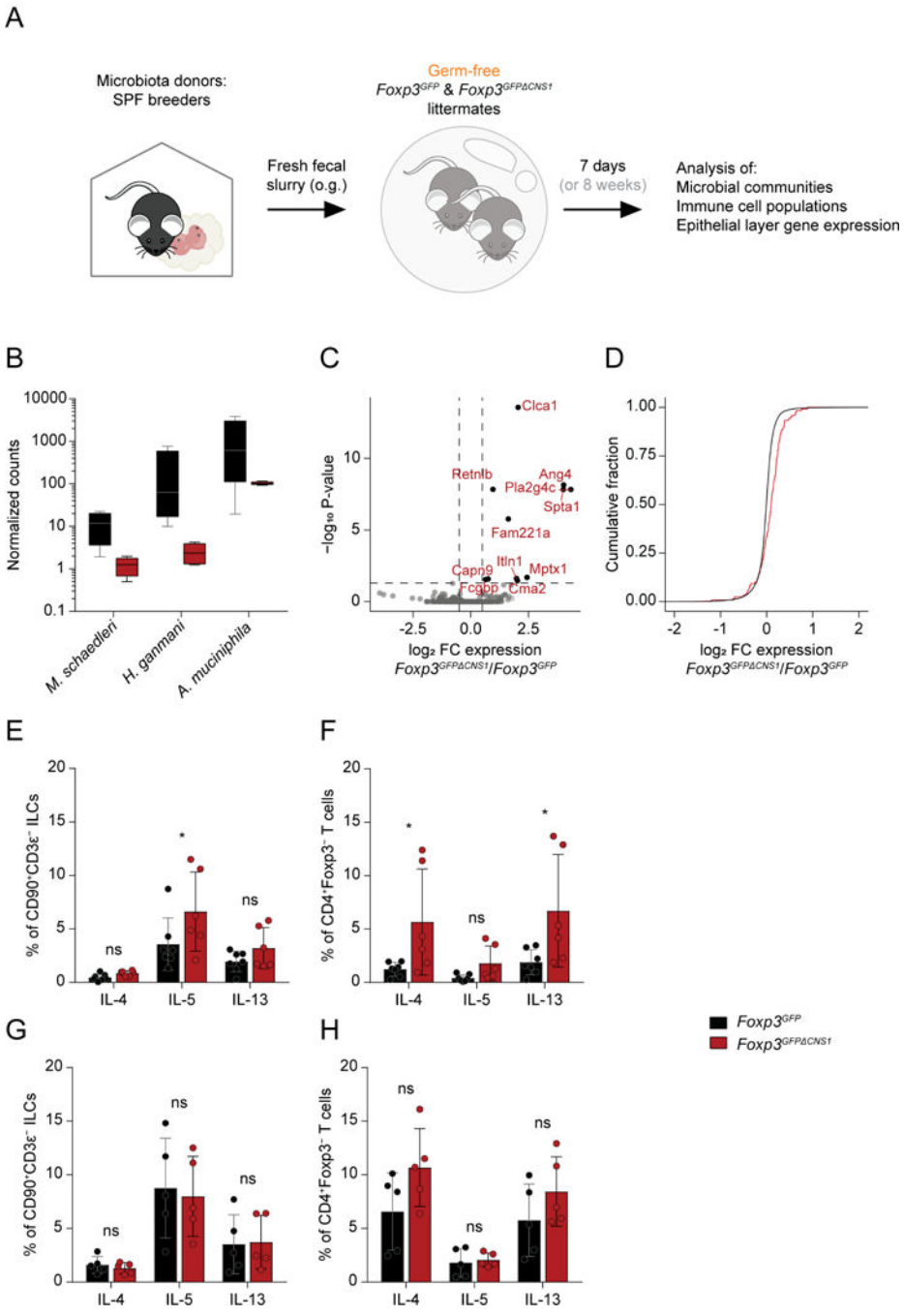

Figure 2. *Foxp3*$^{GFP\Delta CNS1}$ mice mount exacerbated goblet cell and type 2 cytokine responses early after exposure to microbes.

(A) Schematic of experimental design. GF *Foxp3*^{GFP} and *Foxp3*$^{GFP\Delta CNS1}$ mice were gavaged with freshly collected fecal contents from SPF mice and analyzed on D7 post-conventionalization. (B) Fecal DNA was extracted and subjected to 16S rDNA sequencing. Plot shows median and range of normalized read counts associated with the indicated species and are representative of 3 independent experiments (n= 4 mice per genotype). (C-D) RNA-sequencing of the bulk epithelium of the LI of *Foxp3*$^{GFP\Delta CNS1}$ and *Foxp3*^{GFP} mice (n = 4 per genotype). (C) Volcano plots showing $\log_2$ fold-change *Foxp3*$^{GFP\Delta CNS1}$/

Foxp3^{GFP} expression (x axis) and $-\log_{10}$ of P-value (y axis). Significantly altered transcripts (P adj < 0.05) with a $\log_2$ fold-change > 0.5 are shown in red. (D) CDF plot showing cumulative $\log_2$ fold-change across all genes (black) and genes associated with goblet cells (red). Goblet cells genes do not follow the same distribution as all genes (P-value < 1e-10, one-sided ks-test). (E-H) FACS analysis of intracellular cytokine staining after *ex-vivo* re-stimulation. Quantification of the proportion of LI lamina propria cells producing the indicated cytokines in D7 (E, F) and GF (G, H) mice. (E, G) CD3ε$^-$CD90$^+$ ILCs. (F, H) Foxp3$^-$CD4$^+$ T cells. Data in (E-H) are pooled from 2 independent experiments (n = 2–3 mice per group in each experiment). Mean ± SD are plotted. Statistical significance was determined by a two-way ANOVA with Sidak's multiple comparisons correction. *P < 0.05. See also Figure S2.

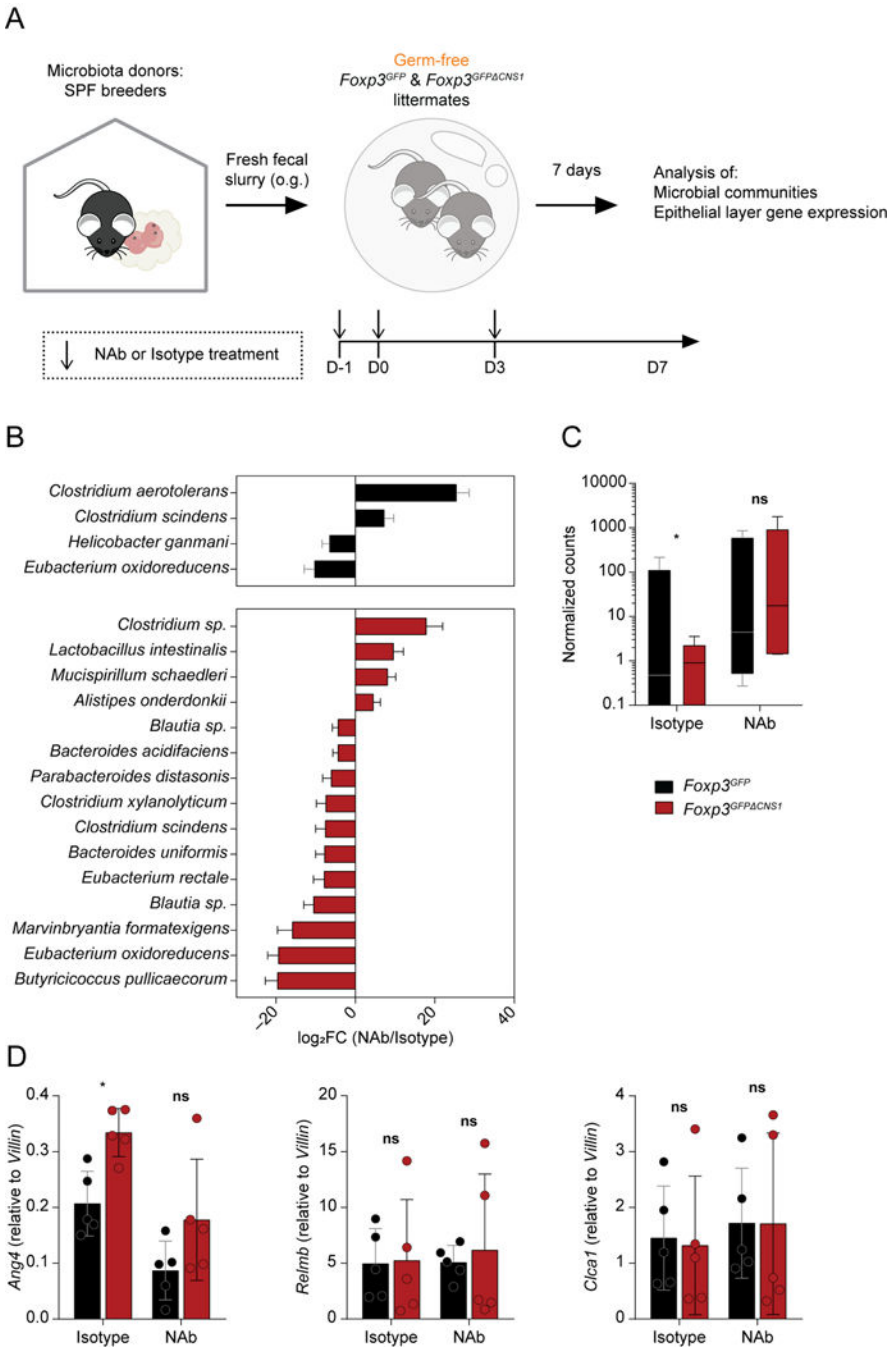

Figure 3. pTreg cells preserve the niche of border dwellers by suppressing type 2 responses during the process of community assembly.

(A) Experimental design scheme. GF *Foxp3*^{GFP} and *Foxp3*^{GFPΔCNS1} mice were injected with neutralizing antibodies against IL-4, IL-5 and IL-13 (NAb) or isotype control, gavaged with freshly collected fecal contents from SPF mice and analyzed on D7 post-conventionalization. (B-C) Effect of NAb treatment on intestinal bacteria. DNA was extracted from fecal pellets and subjected to 16S rDNA sequencing. (B) Bar plots showing $\log_2$ fold-change NAb/Isotype for bacteria significantly affected by treatment in either *Foxp3*^{GFP} (black bars) or *Foxp3*^{GFPΔCNS1} (red bars). (C) Abundance of *M. schaedleri*.

Displaying median with range. Statistical significance for (B-C) was determined by mathematical modeling (see Methods for details). (D) Gene expression analysis of GC-related transcripts by RT-qPCR. Levels of indicated genes in FACS-purified GC were normalized to *Villin.* Statistical significance was determined by a two-way ANOVA with Sidak's multiple comparisons correction. *P < 0.05. See also Figure S3.

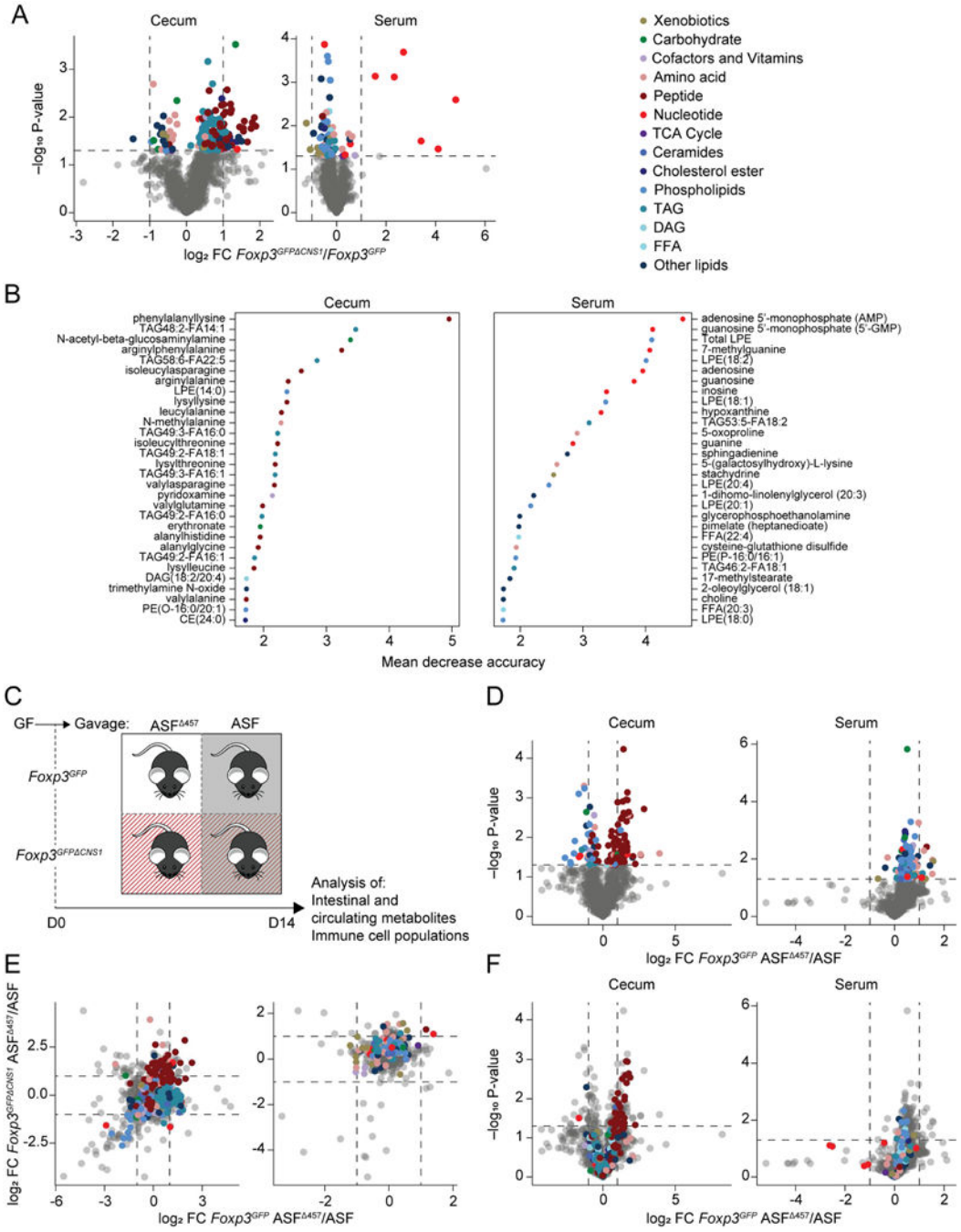

Figure 4. Intestinal and circulating metabolites are affected in pTreg cell-deficient animals.

Serum and cecal contents from SPF *Foxp3*$^{GFP\Delta CNS1}$ and *Foxp3*^{GFP} control mice were subjected to unbiased analysis of polar and non-polar metabolites by LC/MS and DSM/MS, respectively. (A-B) Metabolite analysis in SPF mice. (A) Volcano plots showing $\log_2$ fold-change *Foxp3*$^{GFP\Delta CNS1}$/*Foxp3*^{GFP} (x-axis) and $-\log_{10}$ of p-value (y-axis) for abundance of metabolites detected in the cecum (left panel) and serum (right panel). Significantly different metabolites were colored according to biochemical groups. (B) Random forest analysis for metabolites in the cecal contents (left) and serum (right). (C-F) GF *Foxp3*^{GFP} and

Foxp3$^{GFP\Delta CNS1}$ mice were gavaged with ASF or ASF lacking *M. schaedleri* (ASF$^{\Delta 457}$) consortia and analyzed 14 days after colonization. (C) Experimental scheme of ASF vs. ASF$^{\Delta 457}$ colonization experiments. (D-F) Metabolite analysis in colonized mice. (D) Volcano plots showing $\log_2$ fold-change ASF$^{\Delta 457}$/ASF (x-axis) and $-\log_{10}$ P-value (y-axis) for metabolites detected in the cecum (left panel) and serum (right panel) of wild-type *Foxp3*^{GFP} mice. Significantly different metabolites were colored according to biochemical groups. (E) FC/FC plot showing $\log_2$ fold-change ASF$^{\Delta 457}$/ASF for *Foxp3*^{GFP} mice (x-axis) and $\log_2$ fold-change ASF$^{\Delta 457}$/ASF for *Foxp3*$^{GFP\Delta CNS1}$ mice (y-axis). (F) Metabolites significantly altered in the comparison between SPF *Foxp3*$^{GFP\Delta CNS1}$ vs. *Foxp3*^{GFP} mice (panel A) were colored according to biochemical groups and projected onto volcano plots showing $\log_2$ fold-change ASF$^{\Delta 457}$/ASF for *Foxp3*^{GFP} mice (x-axis) and $-\log_{10}$ of p-value (y-axis) for compounds detected in the cecum (left panel) and serum (right panel). Displaying data pooled from 3 independent experiments (n = 2–3 mice per group). Significance was determined by a MW U-test. Data in panels (A-B) relate to the same animals shown in Figure 1. See also Figure S4.

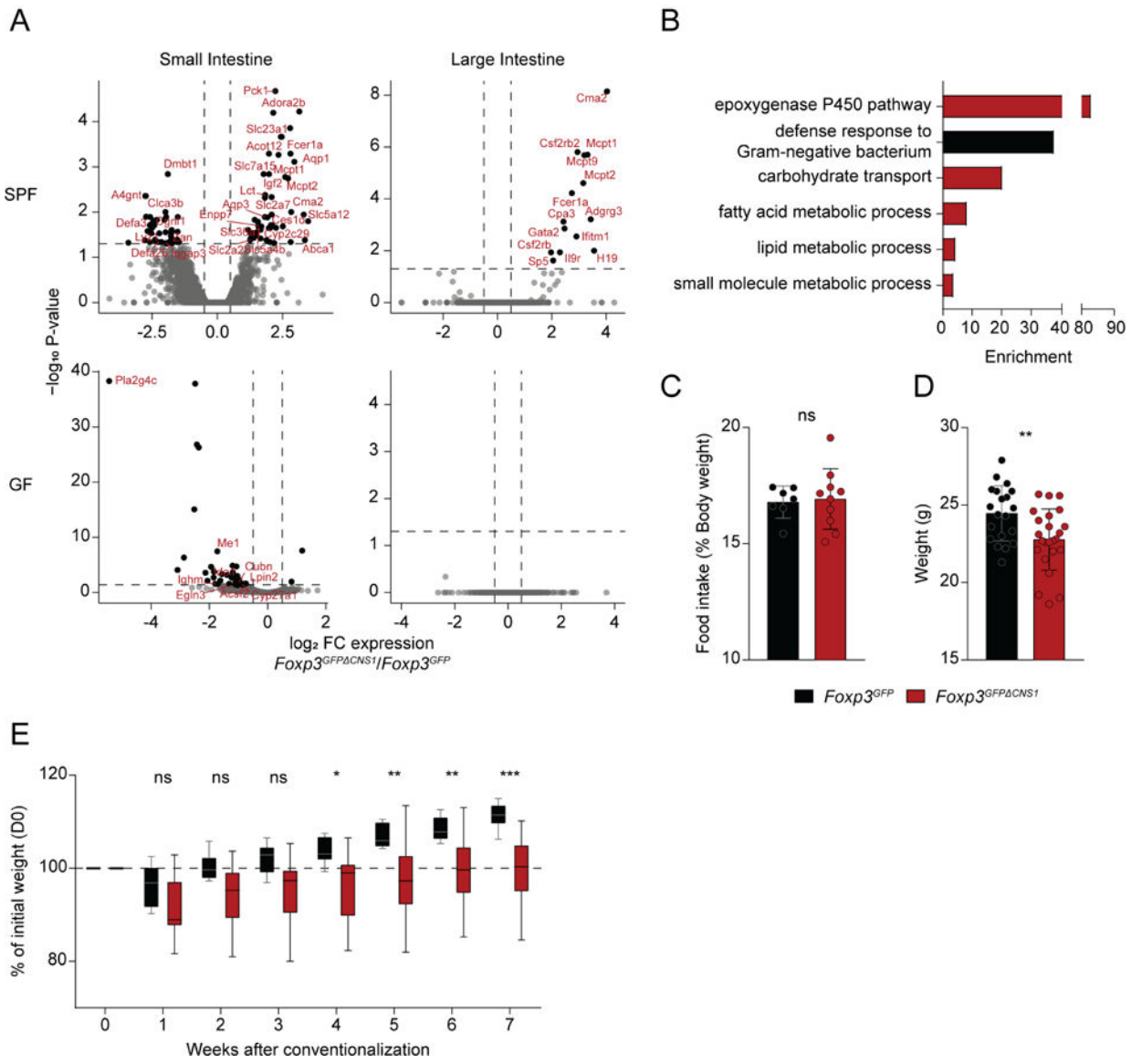

Figure 5. Impaired pTreg cell generation affects intestinal and organismal homeostasis

(A-B) RNA-sequencing of the bulk epithelium of the small (left panel) and large (right panel) intestines from SPF (top) and GF (bottom) *Foxp3*$^{GFP\Delta CNS1}$ and *Foxp3*^{GFP} control mice (n = 2–3 mice per group). (A) Volcano plots showing $\log_2$ fold-change *Foxp3*$^{GFP\Delta CNS1}$/*Foxp3*^{GFP} (x axis) and $-\log_{10}$ of p-value (y axis). Significantly altered transcripts ($p<0.05$) are shown in red. (B) Plot showing Gene Ontology (GO) terms enriched in genes more highly expressed in *Foxp3*$^{GFP\Delta CNS1}$ mice (red) or *Foxp3*^{GFP} mice (black). GO terms with an FDR q-value < 0.05 are shown. Enrichment and q-value were determined by GOrilla. (C-D) Comparison of food intake (C) and body weight (D) between SPF *Foxp3*$^{GFP\Delta CNS1}$ and *Foxp3*^{GFP} mice. Displaying amount of food consumed per 24 hours, normalized by body weight, averaged over 8 days of monitoring. Data pooled from 3 litters (C, n = 7–10) and 6 litters (D, n = 20–24). (E) GF *Foxp3*^{GFP} and *Foxp3*$^{GFP\Delta CNS1}$ mice were gavaged with freshly collected fecal contents from SPF mice and weights were monitored

for 8 weeks. Plot shows weight gain of GF *Foxp3*$^{GFP\Delta CNS1}$ and *Foxp3*^{GFP} mice after conventionalization. Data pooled from 2 independent experiments (n = 4–5 mice per genotype in each experiment). Mean ± SD are plotted (C, D) or Median, quartiles and min/max (E). Statistical significance was determined by a two-way ANOVA with Sidak's multiple comparisons correction. *P < 0.05, **P < 0.01, ***P < 0.001.

Table 1.

Relative levels of selected metabolites in *Foxp3*$^{GFP\Delta CNS1}$ mice.

Serum and cecal contents from SPF *Foxp3*$^{GFP\Delta CNS1}$ and *Foxp3*^{GFP} control mice were subjected to unbiased analysis of polar and non-polar metabolites. Values shown are $\log_2$ fold-change between *Foxp3*$^{GFP\Delta CNS1}$ and *Foxp3*^{GFP} mice. All metabolites are significantly different between groups ($p<0.05$ MW U-test).

Cecum			Serum		
Biochemical	**Class/Pathway**	**$\log_2$FC**	**Biochemical**	**Class/Pathway**	**$\log_2$FC**
phenylalanyllysine	dipeptide	1.85	N-acetyltyrosine	tyr metabolism	−0.53
lysyllysine	dipeptide	1.80	cysteine sulfinic acid	SAM and taurine metabolism	−0.50
histidylalanine	dipeptide	1.66	N-acetylproline	urea cycle	−0.42
arginylvaline	dipeptide	1.57	glutamate	glx metabolism	−0.26
arginylisoleucine	dipeptide	1.55	ornithine	urea cycle	−0.25
arginylleucine	dipeptide	1.55	asparagine	ala and asp metabolism	−0.23
leucylalanine	dipeptide	1.45	aspartate	ala and asp metabolism	−0.22
alanylphenylalanine	dipeptide	1.27	5-oxoproline	glutathione metabolism	−0.16
leucylleucine	dipeptide	1.24	taurine	SAM and taurine metabolism	−0.11
TMAO	phospholipid	0.89	SAH	SAM and taurine metabolism	0.62
TAG54:3-FA20:2	lipid ester	0.40	FFA(20:2)	PUFA	−0.22
TAG56:7-FA20:3	lipid ester	0.89	FFA(20:3)	PUFA	−0.30
TAG56:8-FA20:4	lipid ester	0.85	FFA(20:4)	PUFA	−0.21
TAG52:4-FA22:4	lipid ester	0.66	FFA(22:4)	PUFA	−0.24
TAG58:8-FA22:5	lipid ester	0.79	FFA(22:5)	PUFA	−0.25